ABSTRACT

Title of Thesis:	DEVELOPMENT OF A COMPREHENSIVE PYROLYSIS MODEL FOR FLEXIBLE POLYURETHANE FOAM
	William K. Saar, Master of Science, 2021
Thesis directed by:	Professor Stanislav Stoliarov, Fire Protection Engineering

Flexible polyurethane foams (FPUFs) are polymeric materials which have widespread use and present a large fire risk in modern society. Accurate prediction of their fire behavior is valuable for assessing the risk they pose in any fire scenario they are involved in. Several models have been developed to predict FPUF thermal decomposition at the milligram scale. However, none of these models are able to predict pyrolysis and combustion of gram-sized or kilogram-sized FPUF samples. In this work, a combination of experiments and modeling was used to develop a complete pyrolysis model for a standard FPUF foam. Inverse modeling of thermogravimetric analysis, differential scanning calorimetry, microscale combustion calorimetry, and Controlled Atmosphere Pyrolysis Apparatus II experiments was conducted to obtain a comprehensive list of decomposition reaction kinetics, thermodynamic and transport properties that define the pyrolysis and flaming combustion of this material.

DEVELOPMENT OF A COMPREHENSIVE PYROLYSIS MODEL FOR FLEXIBLE POLYURETHANE FOAM

by

William K. Saar

Thesis submitted to the Faculty of the Graduate School of the
University of Maryland, College Park, in partial fulfillment
of the requirements for the degree of
Master of Science
2021

Advisory Committee:
Professor Stanislav Stoliarov, Chair
Professor Arnaud Trouve
Professor Peter Sunderland
Dr. Isaac Leventon

Acknowledgements

I am lucky to have had many great people in my life during these past two years, all of whom deserve thanks for their support.

Firstly: to my research advisor, Dr. Stanislav Stoliarov. I am truly thankful for the opportunity I have had to work with you during this process. Your mentorship and support have been invaluable. If it were just the knowledge and research experience you had given me, that would be more than enough – but in addition, I have learned so much about quality, work ethic, communication, patience, willingness to help others, and too many other things to mention from the example that you set.

Thank you to my research group and others I've met through the university, for both your help and your friendship: to Conor, Jacques, Dushyant, Ahmed, and Hongen for making me feel welcome and sharing your knowledge; to Lucas, for helping to share the pain of endless setbacks and equipment failure; to Greg, whose previous work has made my life much easier; to Isaac, for both research and general life advice; to Fernando, for all your help in the lab. I'm sure to be missing a few – know that I do truly appreciate you all anyways.

Thank you to Haley, my family, and my friends, who have always given me unconditional support, loyalty, and love. You have all been a tremendous help to me throughout my time in this program and made it much easier to persevere through difficult times.

Thank you to my defense committee members for generously giving their time: Dr. Arnaud Trouve, Dr. Peter Sunderland, and Dr. Isaac Leventon. Thanks to Dr.

Morgan Bruns for assistance with TGA modeling and to Dr. Mauro Zammarano for general help with this research. Finally, I'd like to thank the National Institute of Standards and Technology for their financial support via grant 60NANB19D148.

Table of Contents

List of Tables

List of Figures

List of Symbols

ΔH_r	-	*Heat of reaction*
A	-	*Arrhenius pre-exponential factor*
c_p	-	*Heat capacity*
E_a	-	*Activation energy*
h_{back}	-	*Convective coefficient at the bottom CAPA boundary*
h_c	-	*Heat of combustion*
h_{front}	-	*Convective coefficient at the top CAPA boundary*
k	-	*Thermal conductivity*
m	-	*Mass*
m_o	-	*Initial Mass*
$\dot{q}_{conv.back}$	-	*Convective flux at the bottom CAPA boundary*
$\dot{q}_{conv.front}$	-	*Convective flux at the top CAPA boundary*
$\dot{q}_{rad.back}$	-	*Radiative flux at the bottom CAPA boundary*
$\dot{q}_{rad.front}$	-	*Radiative flux at the top CAPA boundary*
t	-	*Time*
T_{back}	-	*CAPA sample back surface temperature*
α	-	*Absorption coefficient*
ε	-	*Emissivity*
θ	-	*Stoichiometric coefficients*

Chapter 1: Introduction

1.1: Motivation

Residential upholstered furniture (RUF) and mattresses, when ignited, are the two items consistently responsible for causing the most annual home fire deaths in the United States [1]. From 2014 to 2018, home fires in which RUF and mattresses/bedding materials were the first items ignited were responsible for 29% of annual deaths despite accounting for only 3% of reported home fires [1]. Flexible polyurethane foam (FPUF) is widely used as the cushioning in RUF and mattresses [2] and is the key fire load responsible for the extreme fire risk of both items. FPUF's rapid decomposition and high heat of combustion [3] make it likely to disproportionately contribute to flame spread and fire growth in any fire scenario it is involved in. From a life safety perspective, it is clear that the flammability of FPUF is important to understand.

The importance of characterizing FPUF flammability has been recognized in the US for over 50 years. A recent review of the history of FPUF flammability studies [4] provides a picture of the extensive work done in the US to investigate the fire risks of FPUF-related commodities and products. Much of this work, dating back to the first studies of RUF and mattress flammability in the early 1970's, has been in the form of the creation of standardized testing methods [4]. These test methods create criterion for the safe use of FPUF-related products in typical ignition scenarios. For example: California Technical Bulletin # 117 (TB-117) [5] and Consumer Product Safety Commission (CPSC) test #1632 [6], which simulate the ignition by discarded cigarette of upholstered furniture and mattresses, respectively, and assign safety ratings to

products based on the propensity of charring to spread along their surface. Work has also been done to develop practical protection strategies for FPUF, such as the use of fire-resistant barrier fabrics in RUF and mattresses which aim to make ignition of the contained FPUF more difficult [4], and the addition of fire-retardant chemicals to FPUF to reduce its flammability [4]. Though this body of work has led to a better practical understanding of FPUF fire risk and protection strategies, the life safety threat associated with its use still remains. Although the absolute number of annual home fire fatalities caused by RUF and mattresses has decreased from 1984 to 2018, deaths per 1000 reported home fires that began with the ignition of RUF or mattresses have more than doubled [1]. As long as FPUF continues to have widespread use, advancements in the understanding of its flammability have the potential to reduce fire deaths.

1.2: Background

1.2.1: Pyrolysis Modeling

Computational modeling is a modern method for assessing the fire risks associated with a material. Over the past few decades, computational tools which are able to generate predictions of the fire behavior of a material have been developed and significantly advanced. These computational tools provide a viable, cost-effective alternative to standardized physical testing, which as previously mentioned has traditionally been the method by which the fire risk of FPUF is assessed [4]. These tools generally fall into one of two categories: gas-phase computational fluid dynamics (CFD) solvers or condensed-phase pyrolysis solvers. Gas-phase CFD solvers are concerned with predicting the effects of a fire event on a simulated physical space. Their ultimate goal is the accurate prediction of environmental conditions in the

simulated physical space by discrete calculation of heat and mass transfer. Condensed-phase pyrolysis solvers are concerned with prediction of the pyrolysis of a material. Pyrolysis is the thermal decomposition of a condensed-phase (solid or liquid) material into volatile gaseous components. Combustion of these gaseous components is the oxidative chemical reaction which creates the light and heat associated with fire. Given a comprehensive set of material properties and a definition of environmental conditions as inputs, the ultimate goal of a pyrolysis solver is the accurate prediction of the gasification rate of a pyrolyzing material (from which heat release can be calculated). A significant portion of the work done to advance computational fire modeling has been focused on the gas-phase, but it is recognized that an understanding of condensed-phase pyrolysis is critical for capturing ignition and early fire growth [7]. The production of pyrolyzate gasses in polymers is a complicated process and therefore difficult to predict [7], but as computational power has increased, several numerical pyrolysis solvers have been developed. Generally, these pyrolysis solvers operate by solving physical conservation equations of species, energy, and mass at discrete timesteps.

Notably among existing pyrolysis solvers are the solid-phase model of the National Institute for Standards and Technology (NIST) Fire Dynamics Simulator (FDS) [8], Gpyro [9], and ThermaKin [10]. Each of these solvers requires a comprehensive set of thermophysical properties and reaction parameters relating to thermal decomposition and heat transfer as an input. The term ‘pyrolysis model’ will henceforth be used to refer to a complete set of these properties and parameters used as inputs within pyrolysis solver. The goal of this study is to create a comprehensive

pyrolysis model for FPUF capable of accurately predicting its gasification rate by obtaining an accurate set of these properties and parameters, which are further discussed in the following paragraph.

Numerical simulation of the pyrolysis of a material requires a definition of the following: parameters relating to the rate at which each decomposition reaction occurs (reaction kinetics parameters), parameters relating to heat flow to the material as a result of each decomposition reaction (reaction thermodynamics parameters), and certain physical properties of each decomposition reaction component which quantify heat transfer both within the material and to the surrounding environment (thermophysical properties of reaction components). With these three defined in the pyrolysis model, confidence can be had that the predicted temperature of a material based on environmental conditions is accurate, and the gasification rate of the material can be predicted as a function of this material temperature.

1.2.2: Review of Previous FPUF Pyrolysis Studies

The decomposition reaction kinetics of FPUF pyrolysis have previously been studied both for smoldering and flaming combustion. The primary physical difference between the two is the presence of oxygen at the pyrolysis front during smoldering combustion versus the absence of oxygen at the pyrolysis front during flaming combustion. The presence of a flame inhibits oxygen from reaching a material's surface, such that the decomposition occurs anaerobically [11]. In this study, only flaming combustion behavior (anaerobic pyrolysis) was targeted for modeling. Even so, a review of previous FPUF pyrolysis studies includes a brief look at those which

targeted smoldering combustion behavior. It is worth noting that polyurethane foams can vary significantly in chemical structure, and thereby in fire behavior, depending on their formulation [12,13]. 'FPUF' in the context of this study refers only to NIST standard FPUF which was the only foam used for experimentation. In the context of the discussion of other studies, 'FPUF' can refer to polyurethane foams of differing formulations and chemical structures. A description of the NIST standard FPUF and its formulation can be found in section 2.1.

Aerobic Studies

The primary experimental technique by which the reaction kinetics parameters of polymers are investigated is thermogravimetric analysis (TGA). A detailed description of TGA experiments can be found in section 2.2.1. Rein *et al.* [14] conducted TGA experiments and inversely analyzed the results to determine the kinetic and stoichiometric properties of the smoldering combustion of FPUF. A genetic algorithm (a popular tool for the estimation of pyrolysis properties) [15] was used for the inverse analysis to determine the optimal parameters. A 5-reaction n^{th} order scheme was used, which once parameterized was able to successfully capture both the forward and opposed smoldering combustion behavior of FPUF. It should be noted that because reaction thermodynamics and thermophysical properties of reaction components were not measured, energy conservation equations were not solved to determine heat transfer within the foam in the model. Instead, a prescribed temperature distribution based on previous experimental results was assigned ahead of the smoldering front. Dodd *et al.* [16] developed a 7-reaction scheme using Rein *et al.*'s 5-reaction scheme and kinetics parameters as a foundation in order to model two-dimensional smolder propagation

experiments through polyurethane foam using Gpyro [9]. Decomposition reaction kinetics and thermodynamics parameters as well as thermophysical properties of reaction components were optimized by genetic algorithm against the experimental data. More recently, Pau, Fleischmann, and Delichatsios [17] performed TGA experiments differential scanning calorimetry (DSC) experiments (both in air) on both a fire-retarded and non-fire-retarded FPUF. Reaction kinetics parameters were determined by inverse analysis of the TGA data and the overall heat of reaction of the oxidative decomposition at several heating rates was determined by analysis of the DSC data. Unlike the previous studies, a graphical method (inflection point) [18] rather than an optimization algorithm was used to inversely analyze TGA data. A 5-reaction scheme was implemented inside a simplified model developed in the study to reproduce the observed behavior.

Because smoldering combustion kinetics models need to account for both pyrolyzing and oxidative reactions in the condensed phase, they are more complex than flaming combustion models whose reaction schemes only involve thermal decomposition. Rather than the 5- or 7-reaction schemes previously mentioned, most anaerobic FPUF pyrolysis models use a 2-reaction scheme: a decomposition of FPUF into an intermediate component followed by a decomposition of that intermediate component into a residue, with both reactions being accompanied by the release of pyrolyzate gasses. As mentioned earlier, this study aims to capture only flaming combustion behavior and so these anaerobic models are more relevant [11].

Anaerobic Studies

Pau, Fleischmann, Spearpoint, and Li [19] performed anaerobic TGA experiments on both a fire-retardant and non-fire retardant FPUF in order to compare the effects of different inverse TGA analysis methods on resulting reaction kinetics parameters. No attempt at modeling the results was made – rather, the trends of the resulting reaction kinetics parameters achieved by each method were explored. Rather than inversely analyzing the TGA data with a computational model, three different model-free methods of analysis (described by the authors as the kinetic analysis method [20], the Arrhenius plot method [20], and the inflection point method [14]) were used. Similarly, Bilbao *et al.* [21] performed TGA experiments and inversely analyzed the results using a model-free graphical analysis to obtain reaction kinetics properties. The decomposition was categorized into a pre-first, first, and second reaction region. Each region was inversely analyzed separately to determine their reaction kinetics properties. Li *et al.* [22] created 3 variations of a kinetics model for both a fire-retardant and non-fire-retardant FPUF. Anaerobic TGA experiments were performed, and a combination of both mathematical analysis and inverse analysis by genetic algorithm (modeled using Gpyro) were used to determine FPUF reaction kinetics properties. 2 of the model variations used a 2 reaction scheme, while the other used a 3 reaction scheme. The 3 reaction scheme was able to better fit the experimental behavior. In the study most similar to the current one, Prasad *et al.* [23] performed anaerobic TGA experiments to obtain reaction kinetics and microscale combustion calorimetry (MCC) to obtain complete heats of combustion of gaseous components for a non-fire retarded FPUF. A genetic algorithm was used with Gpyro to inversely analyze the TGA data. The kinetic model was used in conjunction with the NIST FDS gas-phase solver to determine the

ability of the kinetic model to reproduce the behavior observed in large-scale FPUF flame spread experiments and cone calorimetry experiments. To enable the modeling of full scale fire behavior, reaction thermodynamics parameters and temperature independent thermophysical properties were estimated from literature values of a generic FPUF formulation. The model was able to recreate the peak heat release rate of the experiments, but significantly overpredicted the rate of flame spread. It qualitatively resembled some experimental behavior but was unable to capture it quantitatively. The authors note that model results are highly sensitive to heats of reaction and recommend the performance of DSC measurements to determine them rather than assignment based on literature values in order to improve model accuracy.

1.3 Objectives and Research Plan

This research attempts to fill several gaps in the current state of anaerobic FPUF pyrolysis modeling. It aims to achieve a more highly validated comprehensive pyrolysis model through the measurement of all three necessary pyrolysis model components – decomposition reaction kinetics parameters, thermodynamics parameters, and thermophysical properties of reaction components – in one study, rather than measurement of some and assignment of literature values to others. This is made possible by a recently developed approach to FPUF pyrolysis model parameterization which is more widely applicable than those used in previous studies. Another important distinction of this study compared to some previous studies is the use of a well-characterized, standard FPUF throughout.

In order to measure the reaction kinetics, reaction thermodynamics, heat release, and heat transfer properties of anaerobic FPUF decomposition, an experimental

and analytical procedure recently developed through a number of studies by Stoliarov *et al.* [24-30] is used. The process involves a hierarchy of milligram- and gram-scale experiments which isolate decomposition processes to enable either the direct measurement or inverse analysis of few pyrolysis-related properties at a time. First, TGA experiments are conducted and inversely analyzed to obtain reaction kinetics parameters (Arrhenius pre-exponential factor (A), activation energy (E_a), and stoichiometric coefficients of reactants and products (θ)). Then, DSC experiments are conducted and, using the kinetic model obtained by analysis of TGA data as a framework, analyzed to determine the heat capacity (c_p) and the heat of each decomposition reaction (ΔH_r). Next, Microscale Combustion Calorimetry (MCC) experiments are conducted which allow for the measurement of the complete heats of combustion (h_c) of all gaseous decomposition products identified from the TGA experiments. Finally, gram-scale experiments (Controlled Atmosphere Pyrolysis Apparatus II [31] are performed to determine heat and mass transport properties as well as optical properties of the FPUF.

An automated approach recently developed by Fiola [32] was used for the inverse analysis of TGA and CAPA II data. Fiola's review of previous pyrolysis model parameterization methods is a good resource for understanding the potential shortcomings of other methods and the need for a revised methodology. ThermaKin2Ds [33,34] is used as the pyrolysis solver throughout this study.

Chapter 2: Methodology

2.1: Material

The chemical structure of polyurethane foams can vary widely based on their formulation. Most generally, they are produced by the reaction of a di-isocyanate and a polyol. In this study, NIST standard FPUF was used for all experiments. NIST standard FPUF is an open cell, polyether-based, TB117-2013 specification compliant [5] foam. It has a composition of 100 parts polyol, 2 parts additives (including surfactants, catalyst, and water), and 43 parts toluene diisocyanate (TDI) and has no added fire retardants. It was measured to have a density of 28.7 ± 0.1 kg m^{-3}.

2.2: Milligram Scale Experiments

2.2.1: Simultaneous Thermal Analysis

A Netzsch Simultaneous Thermal Analyzer (STA) 449 F3 Jupiter was used to conduct all STA experiments. A schematic of the apparatus is shown in Figure 2.1. An STA enables the simultaneous performance of microgram-resolution TGA and DSC experiments in the same apparatus. TGA experiments measure sample mass over a well-defined temperature range at a prescribed heating rate. Characteristics of the decomposition reaction kinetics can be extracted from analysis of these measurements. DSC experiments measure the difference in the amount of heat required to raise the temperature of a sample compared to a known reference. Heat capacities of a sample and its intermediate compositions as well as heats of the thermal decomposition reactions can be estimated by analysis of these measurements.

Several STA experiments were conducted under the following conditions:

- 10 K min^{-1} heating rate
- 313 – 1000 K temperature range
- 4 – 5 mg samples
- 50 mL min^{-1} N_2 flow

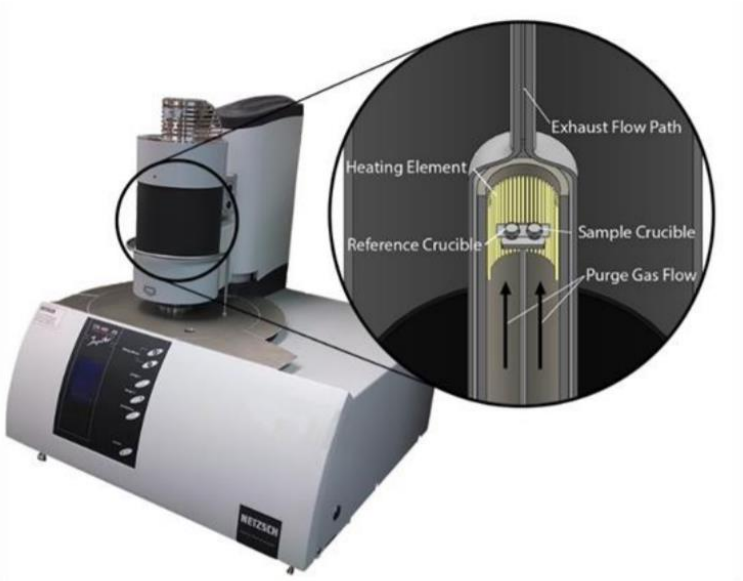

Fig. 2.1. *Netzsch simultaneous thermal analyzer (STA).*

To accumulate necessary statistics and ensure reproducibility, 10 STA experiments were conducted under these conditions using lidded platinum crucibles. The lids covering the crucibles had a small opening in them to release any vaporized foam. Platinum crucibles were chosen for their ability to facilitate good measurements of both TGA and DSC phenomena; it is advantageous to conduct TGA and DSC measurements simultaneously for better correlation of mass loss behavior and corresponding heat flow. Lidded platinum crucibles do however have the potential to affect TGA measurements either by obstruction of pyrolyzate gasses by the lid or by chemical

interaction between the crucible material and sample material. So, to investigate the effect that crucible material and covering might have on TGA results, an additional 3 TGA experiments were performed under the same conditions using open-top ceramic crucibles which are less likely to interact with sample material (ceramic is generally more inert than platinum) or obstruct pyrolyzate transport (no lid). Ceramic crucibles were not used for the main set of STA experiments because they produce poor DSC measurements.

The platinum crucible TGA and DSC data were used to develop the reaction kinetics model and reaction thermodynamics model, respectively, for the FPUF. For use in later model validation, additional open-top ceramic crucible TGA experiments were conducted at 5 and 20 K min^{-1} in triplicate. Once reaction kinetics parameters were determined from the 10 K min^{-1} data, decomposition model predictions were generated at these 5 and 20 K min^{-1} heating rates and compared to experimental data to determine the applicability of the model to a wide range of heating rates.

To investigate the impact of sample preparation method on STA results, FPUF foam powders created by several distinct grinding methods were used (henceforth referred to as ‘machine cryogrinding’, ‘manual cryogrinding’, and ‘manual cryogrinding with additional sieving’). Machine cryoground powder was created using a typical automatic cryogenic grinder. Manually cryoground powder was created using a hand-cranked ceramic grinder which was periodically filled with liquid nitrogen during grinding. The manually cryoground and additionally sieved powder was created using the same method previously described, with the extra step of passing the manually cryoground powder through a 250 μm wire mesh sieve.

2.2.2: Microscale Combustion Calorimetry

Microscale Combustion Calorimetry (MCC) is a standardized test method [35] used to measure the heats of combustion of pyrolyzate gases. These heats of combustion provide a relationship between mass pyrolyzed and heat released. Heats of combustion are the link between the end goal of condensed-phase pyrolysis solvers (prediction of pyrolyzed mass) and the starting point of gas-phase prediction of fire events (heat release). A schematic of the MCC is shown in Figure 2.2. The MCC is generally comprised of 2 sections: a pyrolyzer and combustor. In the pyrolyzer, samples are heated in an anaerobic environment. The pyrolyzate gasses resulting from the heating of the sample travel up a ceramic tube to the combustor, where they are allowed to combust in an air-like environment. By physically separating pyrolysis and combustion, flame heat feedback to the sample surface is eliminated which affords greater control over the temperature of the sample. As a result, the HRR of pyrolyzate gasses can be measured as a function of sample temperature. MCC HRR data was used in conjunction with STA MLR data to determine the complete heats of combustion of pyrolyzate gasses.

All MCC tests (2) were performed under the following conditions:

- 10 K min^{-1} heating rate
- 348 K initial pyrolyzer temperature
- 1023 K maximum pyrolyzer temperature
- 1173 K combustor temperature
- Pyrolyzer environment: 100% N_2
- Combustor environment: 20% O_2, 80% N_2

- Open-top ceramic crucible type

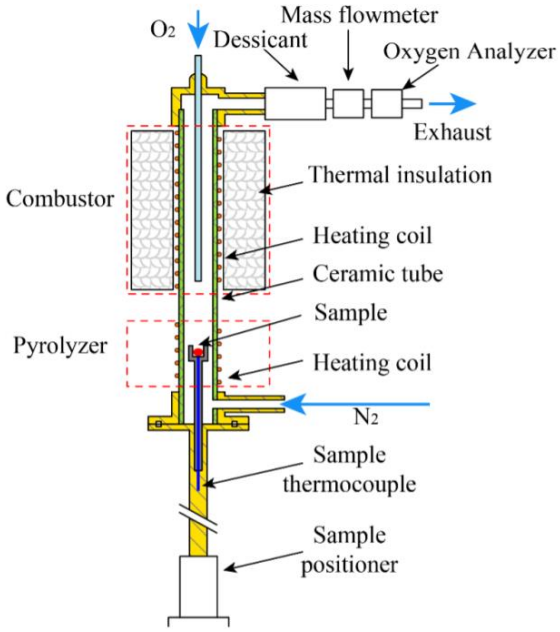

Fig. 2.2. *Microscale Combustion Calorimeter (MCC).*

2.3: Gram Scale Experiments

2.3.1: Controlled Atmosphere Pyrolysis Apparatus (CAPA II)

CAPA II is a custom-designed experimental apparatus which provides well-defined boundary conditions and highly resolved measurements of the mass, temperature, and thickness profile of a non-thermally-thin material exposed to radiant heat [31]. These measurements enable the prediction of thermal conductivity of a material as a temperature-dependent property through inverse analysis of the measurement data. Isometric and cross-sectional drawings of CAPA II are shown in Figures 2.3 and 2.4.

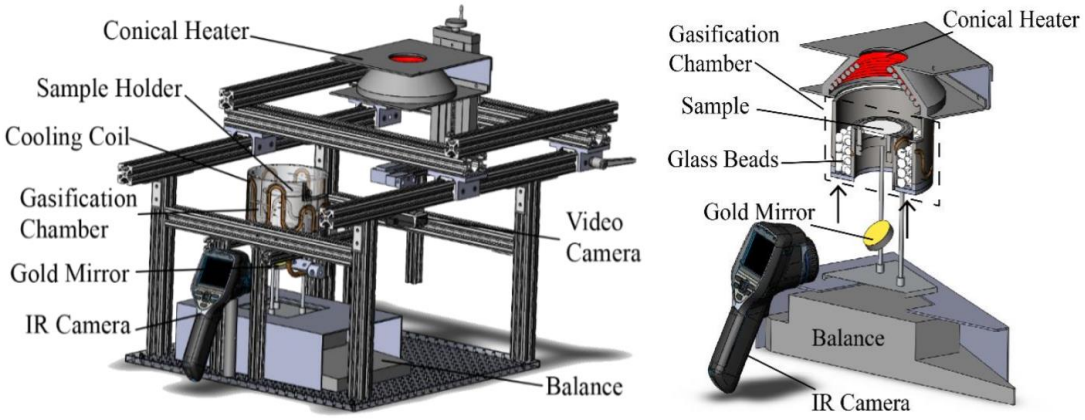

Fig. 2.3. *Isometric drawings of CAPA II.*

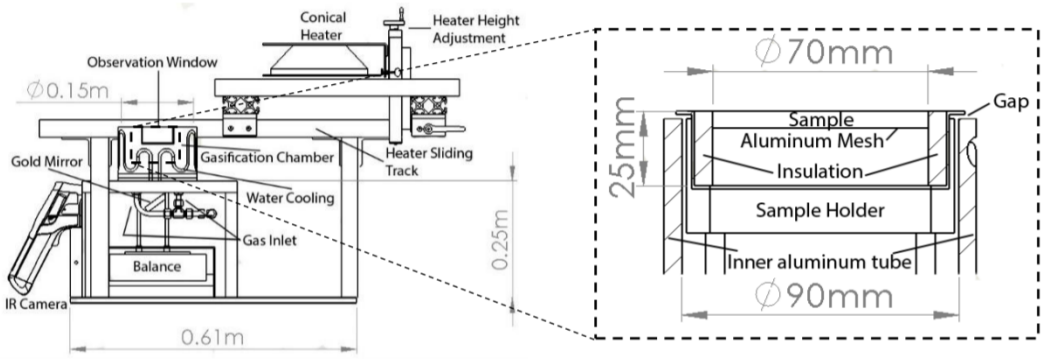

Fig. 2.4. *Cross sectional drawings of CAPA II. Detail of sample holder assembly on right.*

CAPA II is designed to accept samples in the form of 0.07 m diameter disks of variable thickness. These sample disks are held in place by a steel sample holder which can be removed for easier loading and unloading of samples. The sample holder is cylindrical, with an approximate depth of 0.025 m and inner diameter of 0.082 m. Rings of Kaowool PM board insulation were used to insulate the perimeter of each sample from the walls of the sample holder as per Figure 2.4. The sample holder has a 0.07 m diameter hole at its bottom to allow for viewing of the sample from below. The

remainder of the bottom of the sample holder serves as a shelf for the insulation rings. Samples were positioned on top of a piece of 7.6×10^{-4} m thick diamond-shaped aluminum mesh within the sample holder. The aluminum mesh was covered with 2.5×10^{-5} m thick copper foil to support the bottom of the samples and prevent entrainment of ambient air.

During experiments, the sample holder is housed inside the open-to-the-air gasification chamber of CAPA II. The gasification chamber walls consist of two concentric aluminum tubes, each 6.4×10^{-3} m thick. The outer wall extends above the top of the inner wall by 0.02 m. A small section at the top of the outer wall is cut away and replaced with quartz to allow for visual observation of samples during experiments. The inner wall houses the sample holder. Flanges on the sample holder cover the gap between the sample holder and inner gasification chamber wall to reduce ambient air entrainment. The channel between the inner and outer gasification chamber walls can be constantly purged with gas during experiments to maintain a desired atmosphere at the sample surface. To evenly diffuse this gas, the channel is filled with small glass beads 6.4×10^{-3} m in diameter. To maintain more constant and well-defined boundary conditions during experiments, both the inner and outer walls of the gasification chamber are cooled by constantly circulating water through copper tubing which is impressed into channels that run around their exteriors. An electric radiant cone heater capable of delivering up to a 100 kW m^{-2} heat flux is located above the gasification chamber. The bottom edge of the heater is located 0.01 m above the top of the outer gasification chamber wall to reduce air entrainment. The heater is mounted on a sliding

track to enable fast placement to and removal from its position above the gasification chamber.

Three main diagnostics are collected by CAPA II: sample mass, bottom surface temperature, and surface profile. Mass data was recorded by a high resolution (1 mg) Sartorius Cubis mass balance at a frequency of 2 Hz. The sample holder rests on a steel-stilted tray attached to this mass balance. Bottom surface temperature data was recorded by an FLIR E40 infrared (IR) camera focused on the copper foil which supported the sample. The downward-facing surface of the copper foil was coated with a high emissivity ($\varepsilon = 0.92$) paint to ensure the accuracy of the IR temperature measurements. Due to geometric constraints of the apparatus, the IR camera is not able to view the bottom sample surface directly. Instead, its view was directed to the bottom sample surface by an angled gold mirror with an average reflectance of 0.96. The apparent emissivity of the painted copper foil was adjusted in the IR camera to account for the transmission loss of the gold mirror and was validated against thermocouple-based measurements. The surface profile of each sample was captured by a Logitech C930e high definition camera focused on the sample through the quartz observation window in the outer gasification chamber wall. In addition to the sample mass, back surface temperature, and surface profile diagnostics, the temperature of the atmosphere at the sample surface as well as the temperature of the gasification chamber walls were collected to provide more well-defined temperature boundary conditions. Two 1.3×10^{-3} m diameter Type-K thermocouples were used to monitor the inner and outer gasification chamber wall temperatures. A third Type K-thermocouple mounted near

to and flush with the top surface of the sample holder was used to monitor the temperature of the atmosphere at the sample surface.

Several physical characteristics of FPUF and its decomposition make it unique from other materials previously studied using CAPA II, necessitating departures from normal practices:

- FPUF has a density on the order of 50 to 100 times lower than that of materials previously studied with CAPA II. As a result, an atypically large sample thickness was chosen to provide increased sample mass so that calculated experimental mass loss would be more distinguishable from signal noise. Typical sample thicknesses range from 0.64 cm to 1.27 cm. In this study, 1.91 cm thick samples were used.
- FPUF rapidly collapses to roughly $1/30^{th}$ of its initial thickness during decomposition and so spends the majority of each experiment pooled close to the bottom of the sample holder. The heat flux delivered by the cone heater for each experiment was set based on a heat flux gauge measurement taken at the level of the top edge of the sample holder. So, to reduce the distance away from this set point level and thereby the reduction in flux from the setpoint flux that this pool would receive, samples were mounted such that their top surface protruded 0.64 cm above the top edge of the sample holder rather than flush with it. This left the bottom surface of the sample 1.27 cm from the top edge of the sample holder rather than the full 1.91 cm thickness of the sample. Heat flux gauge measurements were conducted at this level to quantify the reduction.

- FPUF decomposition products are liquids at experimental temperatures and will flow. To prevent these decomposition products from leaking or splashing out of the sample holder and potentially damaging parts of the CAPA II assembly, high-temperature fiberglass tape was used to seal the sample holder. The mass loss associated with the decomposition of the tape's adhesive was measured and accounted for in the processing of experimental results.

CAPA II experiments at two different radiant heat flux exposures (25 and 60 kW m^{-2}) were conducted. Each experiment was repeated four times to ensure reproducibility and accumulate necessary statistics. The MLR was computed using a time differential (12 s for 25 kW m^{-2} experiments, 10 s for 60 kW m^{-2} experiments) and normalized by the initial top surface area of the sample. A constant 185 SLPM flow of nitrogen through the gasification chamber was prescribed for the duration of each experiment to maintain an anaerobic atmosphere at the sample surface. Experiments began when the radiant heater was slid into position above a sample and were terminated when either no more mass loss was observed or a sufficiently long time had elapsed without noticeable change to the mass loss rate.

2.4 Modeling

All pyrolysis modeling was performed using ThermaKin2Ds [33,34], the most recent version of the comprehensive pyrolysis solver ThermaKin. ThermaKin2Ds numerically solves mass and energy conservation equations for a condensed-phase object of arbitrary composition undergoing physical and chemical transformations. ThermaKin2Ds was used in a thermally thin (zero-dimensional) mode to analyze the results of milligram-scale tests (TGA, DSC and MCC), and a in a one-dimensional

mode to analyze and predict the results of CAPA II tests. The one-dimensional approximation was determined to be sufficient because the experimental data indicated that both back surface temperature and sample thickness profiles remained nearly uniform in a radial direction for the duration of the CAPA II tests. In all simulations, the gas transfer coefficient was set at 2×10^{-5} m^2 s^{-1} for all gaseous decomposition products, which represents an unimpeded gas flow through the condensed phase. In the CAPA II model, the top sample surface was simulated to have no resistance to gas flow, while the bottom surface was set to be impenetrable to gas flow. All simulations were performed using a 5×10^{-2} mm spatial discretization. Zero-dimensional simulations were performed with a 1×10^{-2} s time step. One-dimensional simulations were performed with a 5×10^{-4} s time step. Increasing or decreasing these integration parameters by a factor of 2 did not produce any significant changes in the simulation results, indicating convergence.

Chapter 3: Results

3.1: Milligram Scale

3.1.1: STA

3.1.1.1: Experimental Results

TGA

Effects of foam powder preparation method were found to be negligible, so the STA data sets of each have been averaged into a single set. There was, however, a notable temperature shift between TGA experiments conducted in platinum and ceramic crucibles, which can be seen in Figure 3.1. Error bars have been omitted for clarity. 'm' and 'm_o' refer to instantaneous and initial mass, respectively.

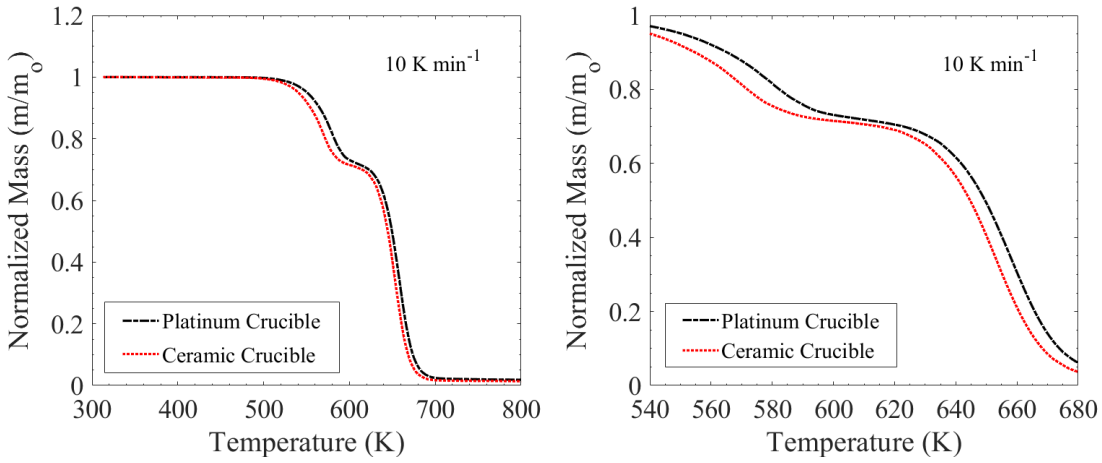

Fig. 3.1. *Averaged normalized mass data for uncorrected platinum and ceramic crucible TGA experiments. Shown on right at reduced temperature range for additional detail of temperature shift.*

An average temperature shift of 6.7 K exists between the two crucible types. For reasons outlined in the methodology, the ceramic crucible TGA data is most likely more representative of the actual physical phenomena – therefore, the platinum crucible TGA data was shifted to match it. This shift is reflected in Figure 3.2.

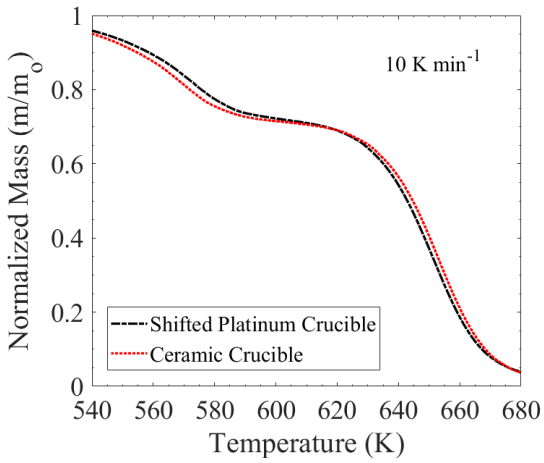

Fig. 3.2. *Averaged normalized mass data from ceramic crucible and shifted (corrected) platinum crucible TGA experiments.*

Corrected normalized mass and MLR data for the platinum crucible experiments are shown in Figure 3.3. All error presented for the remainder of this study is calculated from the scatter of the data as 2 standard deviations of the mean unless otherwise noted. The final residue yield at 800 K, past which there is no significant mass loss, is 1.85 ± 0.05 % wt.

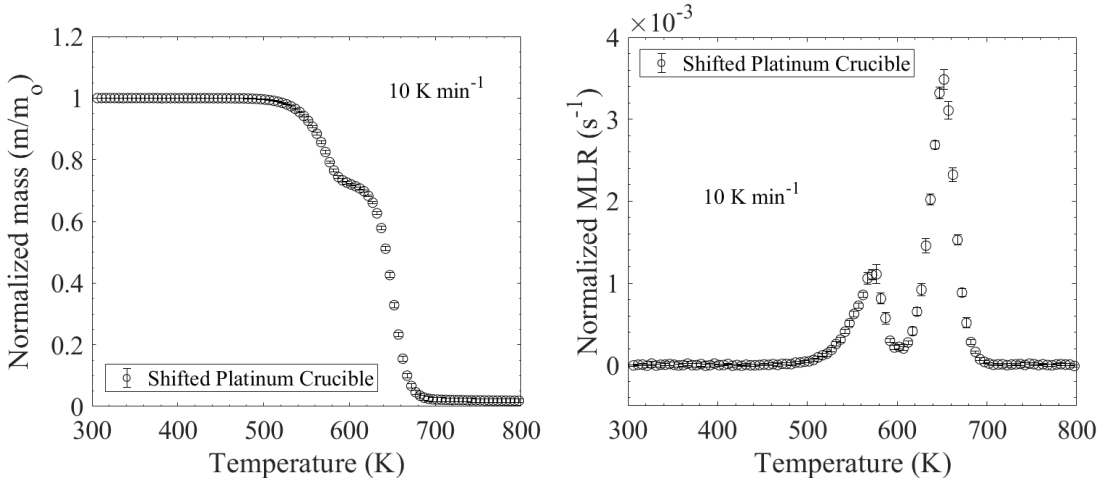

Fig. 3.3. *Averaged corrected normalized mass and MLR data for 10 K min^{-1} platinum crucible TGA experiments.*

DSC

Averaged DSC data for the 10 K min^{-1} STA experiments is shown in Figure 3.4. The same temperature shift described for the TGA data has been applied here. The heat flow and integral heat flow data have both been normalized by initial sample mass. Integral heat flow was computed as the cumulative total heat flow to/from the sample. Positive values indicate an endothermic process.

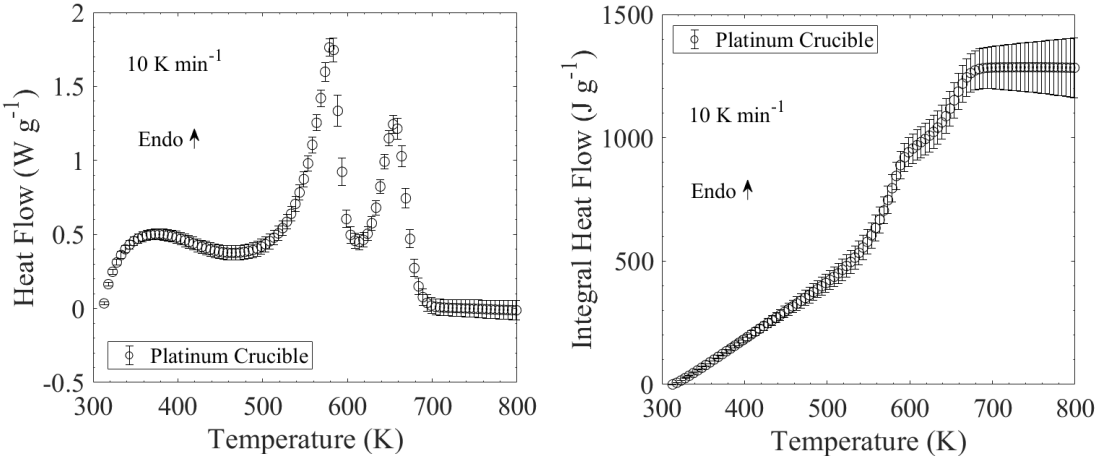

Fig. 3.4. *Averaged heat flow and integral heat flow data for 10 K min^{-1} platinum crucible DSC experiments.*

3.1.1.2: Modeling Framework and Results

TGA Model

The averaged shifted 10 K min^{-1} platinum crucible TGA data was used to determine the kinetics of thermal decomposition. ThermaKin was used to generate modeled TGA data generally based on 2 inputs: a description of the experimental conditions and the reaction scheme associated with the anaerobic decomposition of the sample material.

Defining Model Conditions

An important component of the 'experimental conditions' model input is a definition of the simulated heating rate profile for each experiment. To achieve the most accurate estimation of reaction kinetics properties, the heating rate profile of the simulated experiments should reflect the actual experimental heating rate profiles closely. The heating rate profile of STA experiments is nominally constant but fluctuates in actuality. Transient heating rates as a function of time were empirically derived by examination of averaged experimental time and temperature data for each heating rate and described in ThermaKin with the following exponentially decaying sinusoidal function:

$$\frac{dT}{dt}(t) = a_1\left\{1 - exp\left(-a_2 t\right)\left[cos\left(a_3 t\right) + a_4 sin\left(a_3 t\right)\right]\right\} \quad \text{(Eq. 3.1)}$$

where a_1-a_4 are constants specific to the heating rate.

Table 3.1. *Empirically derived constants for Eq. 1 at each experimental heating rate*

Heating Rate (Test Type)	a_1	a_2	a_3	a_4	*R-square*
5 K/min (STA)	0.0828	0.00298	0.00515	-0.680	0.952
10 K/min (STA)	0.167	0.00302	0.00522	-0.660	0.913
20 K/min (STA)	0.318	0.00308	0.00289	-1.882	0.977
10 K/min (MCC)	0.168	0.00343	-0.00313	0.530	0.912

Constants a_1-a_4 used in Equation 1 for each modeled STA and MCC heating rate profile are shown in Table 3.1. A comparison of experimental transient heating rate and the sinusoidal approximation for the 10 K min^{-1} STA experiments is shown in Figure 3.5. Similar approximations were made for 5 and 20 K min^{-1} heating rates.

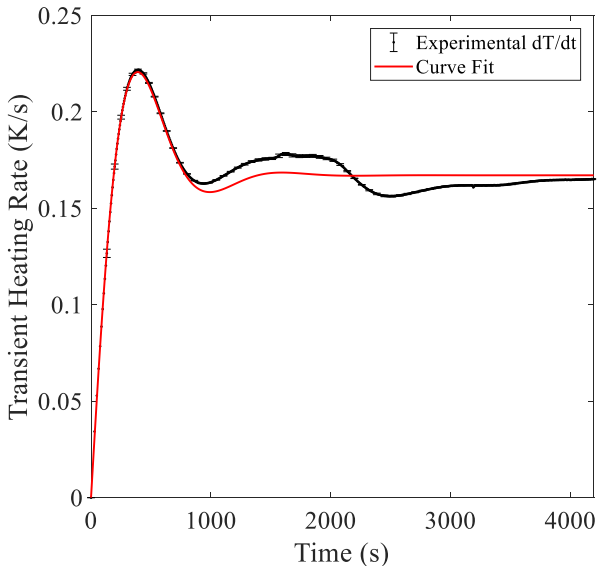

Fig. 3.5. *Transient heating rate vs. time (10 K min^{-1} STA).*

Defining the Reaction Scheme

Definitions of the reaction scheme necessary to generate modeled TGA data include the number of reactions, components present in each reaction, stoichiometric coefficients associated with these components in each reaction, and kinetic properties of each reaction. By defining an appropriate set of reactions and modifying the kinetic properties of Arrhenius equation pre-exponential factor A and activation energy E_a for each reaction, as well as the stoichiometric coefficients associated with each defined component for each reaction, the characteristics of the modeled TGA data can be modified until they agree with experimental TGA data. By this method, the pre-

exponential factor, activation energy, and stoichiometric coefficients of each reaction associated with the thermal decomposition of a material can be estimated.

Based on observation of the experimental TGA data, a reaction scheme involving 2 consecutive first-order reactions was used. A 2 reaction scheme is suggested by the two prominent peaks in the MLR data. The assumption of consecutive first-order reactions was chosen for simplicity, with the goal of capturing the behavior of the experimental data with the minimum number of adjustable model parameters. These consecutive reactions were modeled as:

(1) FPUF → Polyol + Gas $_1$

(2) Polyol → Residue + Gas $_2$

Initially the sample is defined as being composed of entirely FPUF, which in the first reaction decomposes into both an intermediate substance and a pyrolyzate gas. The name used here for the intermediate substance is ‘Polyol’. Other researchers have used ‘Polyol’ to refer to an intermediate product of the thermal decomposition of FPUF foam [14,16,17,19,21-23] with the justification that a re-separation of FPUF foam into TDI and polyol, the two primary ingredients used in the formation of FPUF foams, is a good approximation of the actual decomposition [36]. No assertion about the chemical makeup of the intermediate product is made here, but the name polyol is adopted. In the subsequent reaction, the intermediate decomposes into a final residue and another pyrolyzate gas.

Model Results

Initial estimations and subsequent optimization of the pre-exponential factor *A*, activation energy E_a, and stoichiometric coefficients were obtained using an in-house optimizer which employed recursive execution of ThermaKin simulations and a hill-climbing algorithm [32] until modeled TGA data most matched experimental TGA data. The goodness of fit (*GoF*) criterion used as the target for the optimization was as described in Equation. 3.2:

$$GoF = 1 - \frac{1}{Exp_{max}} \sqrt{\frac{\sum_{i=1}^{N} (Exp_i - Model_i)^2}{N}} \qquad \text{(Eq. 3.2)}$$

where *Exp* indicates experimental values, *Model* indicates model values, *N* is the number of experimental data points, and Exp_{max} is the maximum experimental value. The squared difference between experimental and model values at each experimental data point is summed and normalized by both the number of data points and the maximum experimental value. More information can be found in Fiola's thesis [32].

A comparison of the optimized 10 K min^{-1} model and experimental 10 K min^{-1} data can be seen in Figure 3.6. Optimized kinetic parameters of each reaction can be seen in Table 3.2. All stoichiometric coefficients presented are mass based.

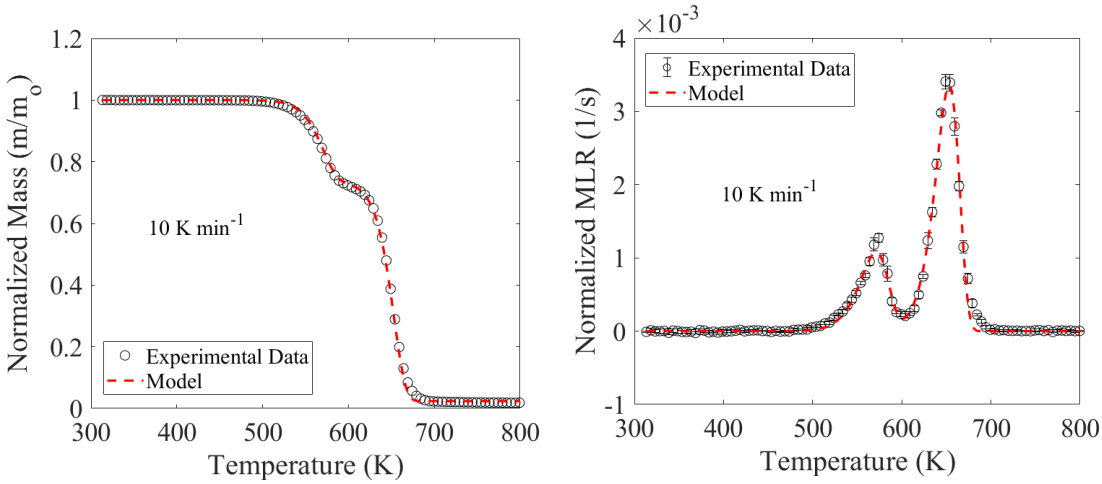

Fig. 3.6. *Comparison of 10 K min^{-1} ThermaKin TGA model with experimental data.*

Table 3.2. *Optimized Reaction Kinetics*

Reaction	*A* (s^{-1})	E_a (kJ mol^{-1})	*Stoichiometry*
1	2.45×10^{13}	168	**FPUF → 0.733 Polyol + 0.267 Gas** $_1$
2	9.59×10^{18}	262	**Polyol → 0.033 Residue + 0.967 Gas** $_2$

Reaction Model Validation

To verify the model's ability to accurately predict the thermal decomposition of the FPUF across a range of heating rates, predictions were generated using the optimized reaction scheme at 5 and 20 K min^{-1} heating rates and compared to experimental TGA data (fig. 3.7 & 3.8). The 5 and 20 K min^{-1} TGA data was collected using open-top ceramic pans and was not temperature shifted. There is good agreement between model prediction and experimental data for both additional heating rates which

provides confidence that this thermal decomposition model is valid over a wide range of heating rates.

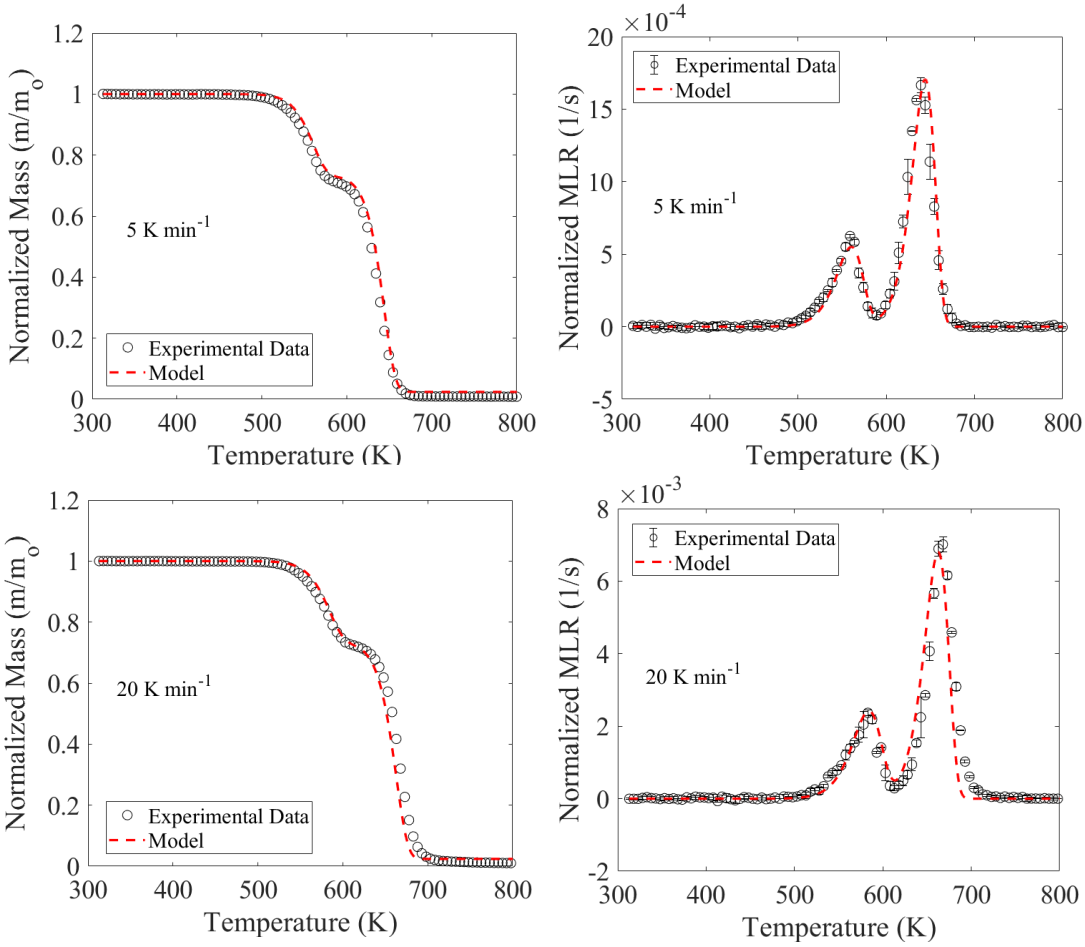

Fig. 3.7. *Comparison of 5 K min^{-1}(top) and 20 K min^{-1} (bottom) ThermaKin model outputs with experimental data.*

Comparison to existing models

As mentioned in section 1.2, several anerobic reaction kinetics models for FPUF foam have been previously developed by other researchers [17,19,21-23]. A selection of these have been included here for comparison. A comparison of the normalized MLR profiles of these selected models with those of this newly developed model at both 5

and 20 K min^{-1} heating rates is shown in Figure 3.8. There is good agreement between this model and Bruns and Leventon's model, and to a lesser degree Li *et al.*'s and Pau *et al.*'s model. The similarity to Bruns and Leventon's model is likely due to the fact that we studied the same foam. The thermal decomposition behavior of foams can vary greatly due to small changes in composition [12,13], and in this way any similarity or discrepancy between models is potentially explained by similarities or discrepancies in the composition of the foams studied to develop them. However, not enough information exists about the composition of the foams Li *et al.* and Pau et. al studied to say with certainty how close or far their formulations were from the FPUF used in this study. Each model included here for comparison is generally in agreement about the temperature at which the MLR onset and peaks occur for both reactions. The magnitude of the MLR peaks of each reaction, particularly the second, show less agreement between models.

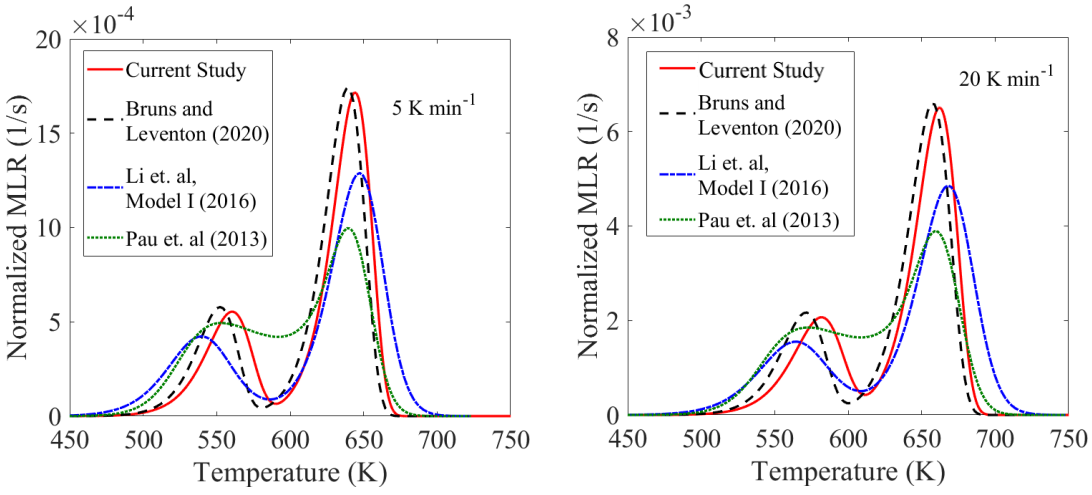

Fig. 3.8. *Comparison of 5 and 20 K min^{-1} model output with previously developed kinetics models.*

DSC Model

With the thermal decomposition model parameterized, ThermaKin could be used to generate modeled DSC data. The modeled DSC conditions were identical to those previously described in the TGA model conditions section, as the DSC experiments occurred simultaneously with the 10 K min^{-1} TGA experiments in the same apparatus. Adjustable parameters in the DSC portion of the ThermaKin model correspond to the heat of each reaction ΔH_r and the heat capacity c_p of each condensed-phase reaction component. The process for optimizing these parameters was divided: first, the heat capacity of each component was estimated to determine a sensible enthalpy baseline - then, heats of each reaction were determined.

The sensible enthalpy baseline was determined by approximating heat flow into the sample in the absence any of chemical reactions, which was represented in the ThermaKin model by a zero-value assigned to the heat for each reaction. This baseline was altered by modifying the heat capacities of each component until it best matched the heat flow DSC data with reaction heat peaks disregarded. This method was used to determine heat capacities of the virgin FPUF foam and final residue but was made somewhat difficult for the intermediate Polyol by the proximity of the first and second reaction peaks, which obscure the experimental baseline. To overcome this obscuration, heat capacity of the Polyol was approximated in several ways: as equivalent to the heat capacity of the virgin FPUF foam, final residue, and an average between the two. Of the three methods, equating the heat capacity of the Polyol with that of the virgin FPUF foam produced the best results. Once the sensible enthalpy baseline was determined, the heats of each reaction were modified until the modeled

heat flow and integral heat flow data best agreed with experimental data. A comparison of modeled and experimental heat flow and integral heat flow data is shown in Figure 3.9. Resulting heats of reaction and heat capacities of each component are shown in Table 3.3 and 3.4

Table 3.3. *Optimized Heats of Reaction*

Reaction	ΔH_r (J kg^{-1})
FPUF → Polyol + Gas 1	-3.7 x 10^5
Polyol → Residue + Gas 2	-3.3 x 10^5

Table 3.4. *Optimized Heat Capacities*

Component	*Heat Capacity* (J kg^{-1} K^{-1})
FPUF	2250
Polyol	2250
Residue	2000

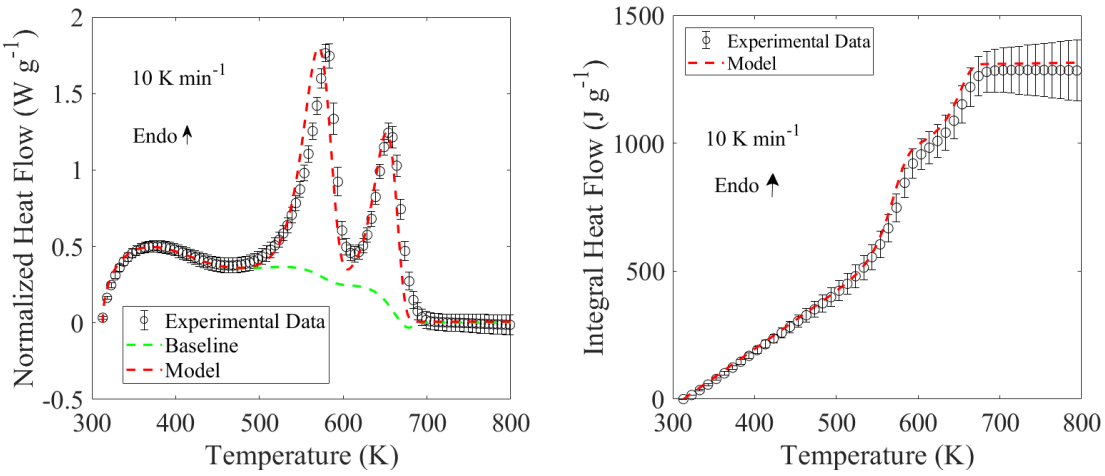

Fig. 3.9. *Comparison of 10 K min^{-1} DSC experimental data with ThermaKin predictions.*

3.1.2: MCC

Averaged results of the 2 MCC experiments are shown in Figure 3.10. Error bars are calculated as the difference between individual and mean experimental HRR at each temperature. Integral HRR was computed as the cumulative total heat release rate from the combustion of the pyrolyzate gasses. Both HRR and Integral HRR have been normalized by initial sample mass.

The heats of complete combustion h_c for the pyrolyzate gas produced in each of the 2 modeled reactions were determined by simulation of the MCC data. A small HRR peak occurring at around 575 K suggests the presence of a third reaction not captured by TGA or DSC experiments, but which for the purposes of this model is not significant enough to warrant trying to capture. Using an experimentally derived heating rate profile specific to the MCC experiments (as detailed in section 3.1.1.2) and the reaction scheme and component parameters previously determined for the thermal decomposition model, simulated MLR profiles for each reaction were generated. Simulated HRR profiles were achieved by scaling these MLR profiles by constants which corresponded to the heats of complete combustion of each pyrolyzate gas until the best agreement between modeled and experimental results were achieved.

An initial comparison of modeled and experimental HRR profiles revealed a notable temperature shift between the two at the onset of the first reaction. This type of discrepancy is not unprecedented in modeled MCC HRR profiles [37]. Any significant heat release should require concurrent mass loss – therefore, the discrepancy was attributed to sample temperature deviations measured by the MCC thermocouple and the experimental HRR profiles were shifted to a higher temperature. The profiles were

shifted in such a way as to balance the discrepancy between the first and second reactions and best match experimental and modeled HRR peak temperatures. The magnitude of this shift was approximately 9 K. The final optimized heats of complete combustion of both pyrolyzate gas species was 28 kJ g^{-1}. Original and shifted experimental HRR profiles as well as the model HRR profile are shown in Figure 3.10.

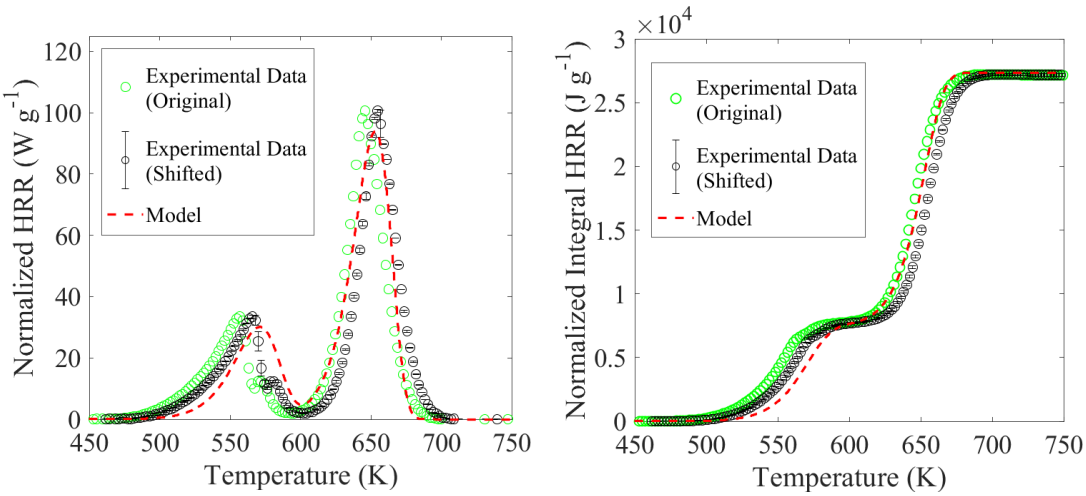

Fig. 3.10. *Original experimental, shifted experimental, and modeled HRR and Integral HRR profiles for 10 K min^{-1} MCC experiments*

3.2: Gram Scale

3.2.1: CAPA

3.2.1.1: Experimental Results

Average MLR and back surface temperature T_{back} results of the 4 CAPA experiments at each heat flux exposure are shown in Figures 3.11-3.12 and 3.14-3.15. All error presented was calculated as 2 standard deviations of the scatter of the data. Average normalized sample mass for each heat flux exposure is shown concurrently (without error bars for clarity) with the MLR and T_{back} results. MLR was calculated

as a 12 second time differential for the 25 kW m^{-2} experiments and a 10 second time differential for the 60 kW m^{-2} experiments – the minimum differentials that produced clean features in the data. MLR is presented per unit area (PUA), normalized by the initial area of the top sample surface. To better understand a discussion of the presented results, it is helpful to see the unique physical decomposition of the FPUF CAPA samples. Annotations made on Figures 3.11-3.12 and 3.14-3.15, labeled chronologically, correspond to significant features of the results. Concurrent sample photos and feature descriptions accompany these annotations (Fig. 3.13 and 3.16).

Different MLR behavior is observed at each experimental heat flux. At the 25 kW m^{-2} exposure, a single MLR peak at 27 s with a ~140 s decay to a steady low value is present. Mass is lost at a relatively constant, very low rate throughout the remainder of the experiment following the peak. At the 60 kW m^{-2} exposure, 2 sharp peaks at 6 s and 43 s are present. The second has a ~110 s decay to a steady low value, after which mass is lost at a constant near-zero rate.

The T_{back} behavior at both fluxes is unusual. At the 25 kW m^{-2} exposure, T_{back} reaches a peak at 150 s and slowly declines for the remainder of the experiment. At the 60 kW m^{-2} exposure, a local peak and trough occur at 21 s and 25 s, respectively. These are followed by an increase to a temperature peak at 43 s and subsequent temperature decline. Given enough time (~700 s), T_{back} begins to rise again in 60 kW m^{-2} experiments. This eventual rise coincides with a reduction in MLR from the near-zero constant value described before to an actual value of zero. In previous CAPA II studies, back surface temperature has not decreased at any point during experiments [27-32].

At both heat fluxes, samples collapse into a shallow pool (with a depth on the order of 1 mm) relatively quickly. This collapse was fully achieved as quickly as 73 s after exposure at 25 kW m^{-2} and 19 s after exposure at 60 kW m^{-2}.

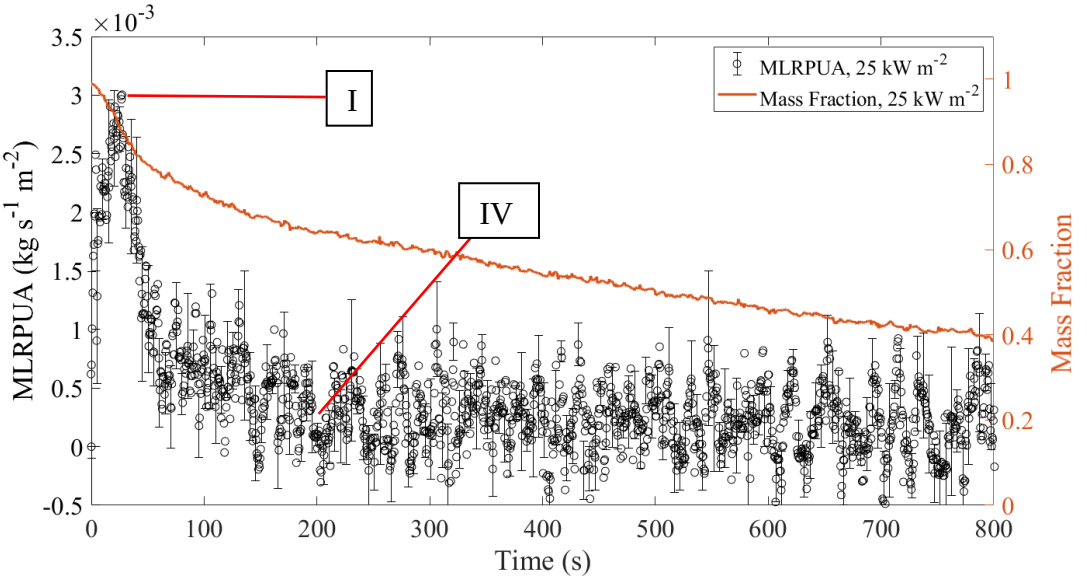

Fig. 3.11. *Average mass loss rate per unit area of the 25 kW m^{-2} CAPA experiments.*

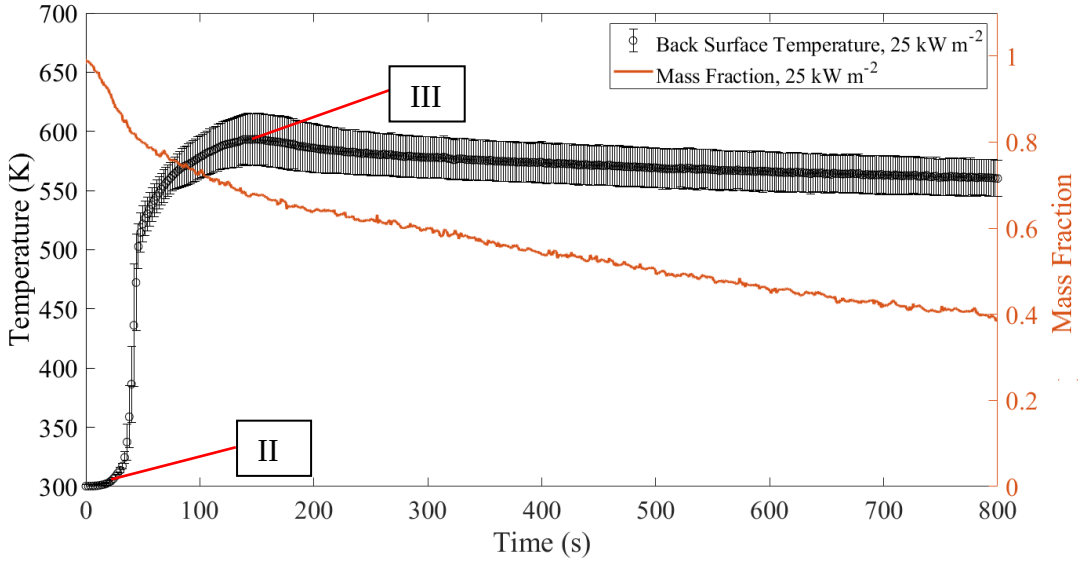

Fig. 3.12. *Average back surface temperature of the 25 kW m^{-2} CAPA experiments.*

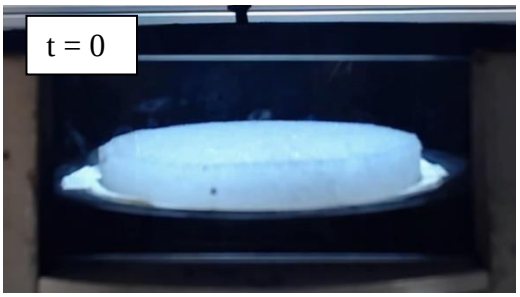

(0 s) First image after 25 kW m^{-2} exposure.

(27 s) MLRPUA reaches peak value (3.0 × 10^{-3} ± 5 × 10^{-4} kg m^{-2} s^{-1}). Sample has collapsed to approximately ½ of its original thickness. Bubble beginning to form at center of sample.

(33 s) Onset of rapid temperature increase. The bubble at the center of the sample has fully formed and begins to collapse.

(150 s) Back surface temperature (T_{back}) reaches peak of 594 ± 22 K. After this time, T_{back} slowly declines for the remainder of the experiment (reaches 550 ± 15 K at 1800 s)

(165 s) MLRPUA drops from peak value to relatively steady low value for remainder of experiment.

Fig. 3.13. *Visual timeline of 25 kW m^{-2} CAPA experiments.*

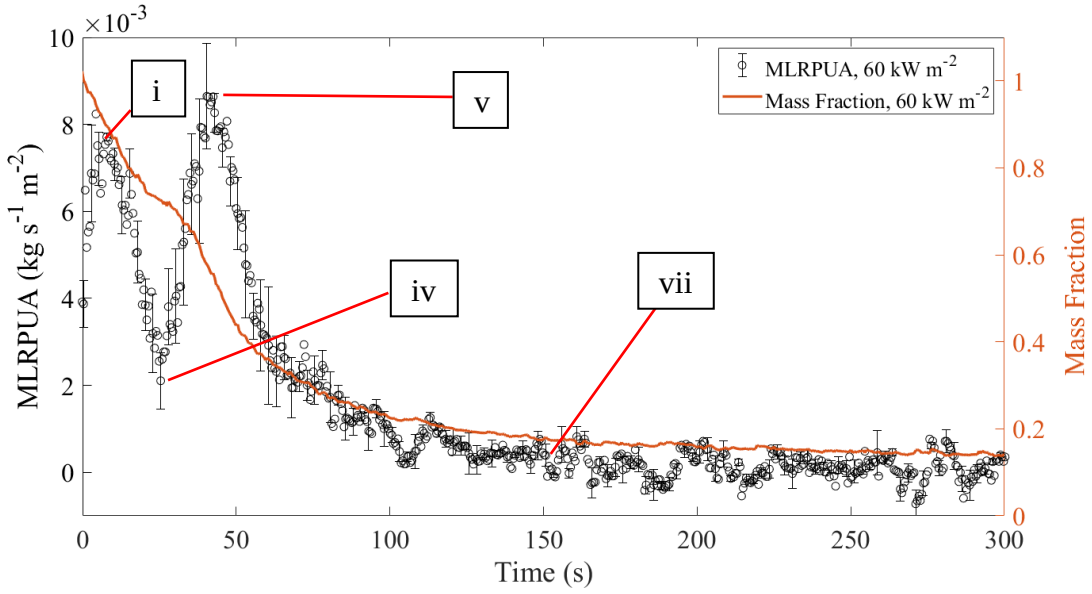

Fig. 3.14. *Average mass loss rate per unit area of the 60 kW m^{-2} CAPA experiments.*

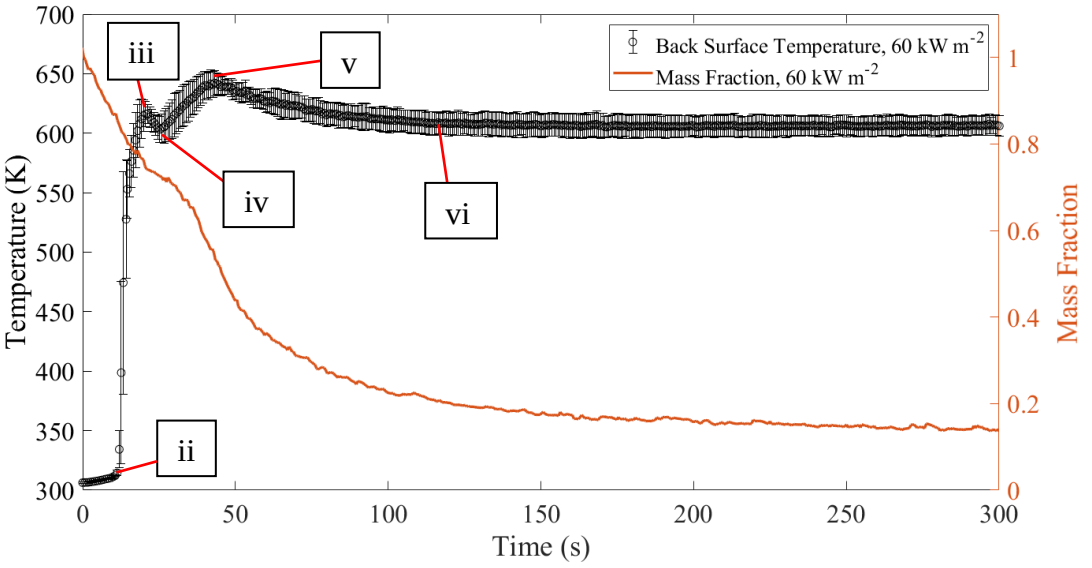

Fig. 3.15. *Average back surface temperature of the 60 kW m^{-2} CAPA experiments.*

(0 s) First image after 60 kW m^{-2} exposure.

(6 s) First mass loss peak ($8.2 \times 10^{-3} \pm 7 \times 10^{-4}$ kg s^{-1} m^{-2}). Sample has collapsed to approximately ½ its original thickness. Bubble beginning to form at center of sample.

(11 s) Onset of rapid temperature increase. Bubble has nearly fully formed and begins to collapse 1-2 s later.

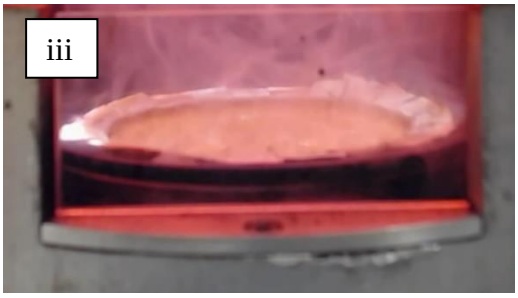

(21 s) T_{back} reaches local maximum (617 ± 8 K) and starts to decline. Sample has collapsed to near bottom of sample holder, but vapors make it hard to see any details.

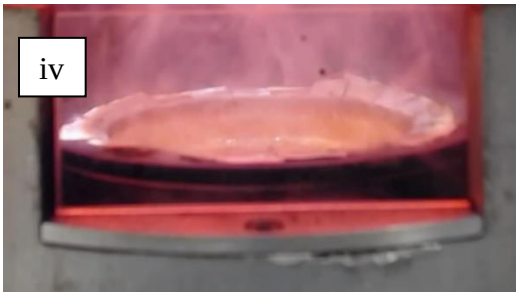

(25 s) MLRPUA and T_{back} simultaneously reach local minimums (MLRPUA = $2.1 \times 10^{-3} \pm 7 \times 10^{-4}$ kg s^{-1} m^{-2} , T_{back} = 603 ± 11 K) and start to increase.

Fig. 3.16. *Visual timeline of 60 kW m^{-2} CAPA experiments*

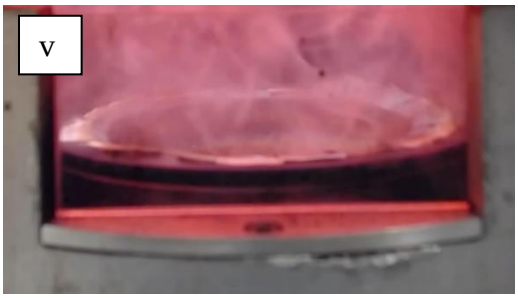

(43 s) MLRPUA and T_{back} simultaneously reach maximums (MLRPUA = $8.6 \times 10^{-3} \pm 1.2 \times 10^{-3}$ kg s^{-1} m^{-2}, T_{back} = 642 ± 11 K) and begin to decline.

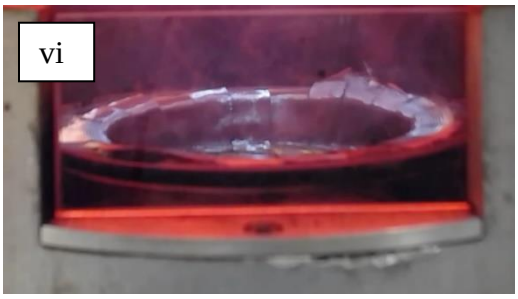

(~150 s) T_{back} reaches steady low value (608 ± 9 K)

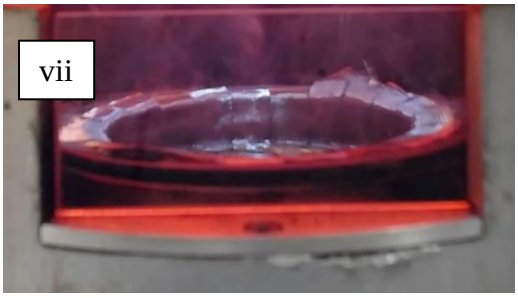

(~160 s) MLRPUA reaches steady low value

Fig. 3.16 (cont.) *Visual timeline of 60 kW m^{-2} CAPA experiments*

3.2.1.2: Modeling Framework and Results

Defining Model Conditions

The CAPA experiments were modeled using ThermaKin2Ds in a one-dimensional mode. In this configuration, the model is defined by front (top) and back (bottom) boundary conditions.

Front Boundary

The front boundary of the CAPA model was defined by both a radiative and convective heat flux. To understand the definition of the modeled radiative flux, a review of CAPA experimental procedures and observations is helpful.

Before each experiment, the cone heater is set to deliver the desired flux based on a heat flux gauge measurement conducted at the level of the top edge of the sample holder – the 'setpoint height'. The nature of the decomposition of the FPUF foam, however, causes the exposed surface of the sample to remain at this setpoint height for only a brief period; it is 0.64 cm above the setpoint height at the beginning of the experiments and collapses to the bottom of the sample holder 1.27 cm below the setpoint height in as few as 19 s after exposure at 60 kW m^{-2} and 73 s after exposure at 25 kW m^{-2}. The ThermaKin model can accurately predict any increased flux due to the sample surface being higher than the setpoint height but cannot accurately predict decreased flux due to sample surface being lower than the setpoint height. Therefore, this decreased flux was prescribed. The radiative model flux was thusly configured as an initial constant flux corresponding to the nominal radiant heater setting for each experiment, followed by a prescribed downwards ramp concurrent with the experimentally observed times at which the sample reached the setpoint height and bottom of the sample holder. This lower flux remained for the duration of the simulation. The magnitude of the decrease in heat flux was found to be approximately 8-9% of the setpoint flux, or 2 kW m^{-2} for the 25 kW m^{-2} experiments and 5 kW m^{-2} for the 60 kW m^{-2} experiments.

The convective flux at the top boundary $\dot{q}_{conv.front}$ was calculated by ThermaKin based on a definition of the environmental temperature around the top sample surface $T_{gas.front}$ and a radially dependent convection coefficient h_{front}.

During experiments, the environmental temperature was measured by a thermocouple positioned in the nitrogen flow directly above the glass beads. The measured temperature profile was described in the ThermaKin model by the following equation:

$$T_{gas.front} = C_1\, e^{C_2 t} + C_3 e^{C_4 t} + T_{HFG} \qquad \text{(Eq. 3.3)}$$

where $C_{1\text{-}4}$ are coefficients resulting in the best fit of experimental data, T_{HFG} is the temperature of the water used to cool the heat flux gauge with which the radiant heater was set, and *t* is time after exposure to the radiant heater.

h_{front} was described in the ThermaKin model by Eq 3.4:

$$h_{front} = e_1 \left(\frac{r_z}{R}\right) + e_o \qquad \text{(Eq. 3.4)}$$

Where e_1 = 8.45 W m^{-2} K^{-1}, e_o = 2.97 W m^{-2} K^{-1}, R is the radius of the CAPA II sample, and r_z is the radial position at which the convective coefficient is being calculated. This relationship was determined in a previous study of CAPA II heat transfer [31].

Convective flux to the top surface of the sample $\dot{q}_{conv.front}$ was defined in the ThermaKin model by Eq. 3.5:

$$\dot{q}_{conv.front} = h_{front}(T_{gas.front} - T_{front}) \qquad \text{(Eq. 3.5)}$$

Modeled vs. averaged experimental gas temperature profiles as well as coefficients for each model profile are shown in Figure 3.17 and Table 3.5.

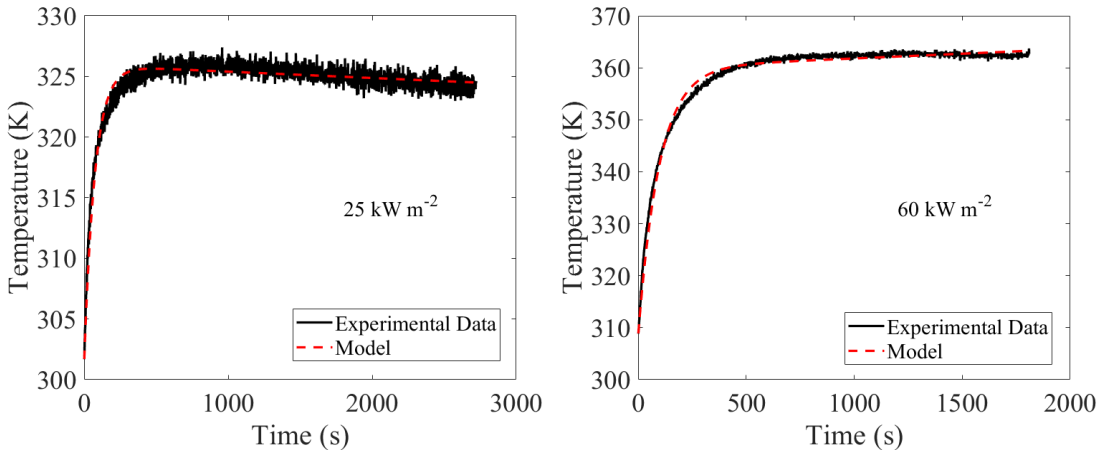

Fig. 3.17. *Modeled vs. experimental CAPA $T_{gas.front}$ profiles for 25 kW m^{-2} experiments (left) and 60 kW m^{-2} experiments (right).*

Table 3.5 *Model CAPA gas temperature coefficients.*

Heat Flux	C_1 [K]	C_2 [K s^{-1}]	C_3 [K]	C_4 [K s^{-1}]	T_{HFG} [K]
25 kW m^{-2}	32.9	-1.6 × 10^{-5}	-24.5	-0.013	293
60 kW m^{-2}	67.0	2.64 × 10^{-5}	-51.6	-0.01	293

Back Boundary

The back boundary of the CAPA model was also defined by a radiative and convective heat flux, $\dot{q}_{rad.back}$ and $\dot{q}_{conv.back}$. The definition of both fluxes was based on the measured experimental temperature profile of the inner CAPA II wall facing the sample. It was assumed that the temperature of the gas in the vicinity of the back sample

surface is equal to the temperature of the wall. This temperature, $T_{gas.back}$, was modeled as a linear ramp and constant hold, as shown in Figure 3.18, and related to the back surface heat fluxes as per Equations 3.6 and 3.7:

$$\dot{q}_{rad.back} = \varepsilon\sigma(T_{gas.back}^4 - T_{back}^4) \qquad \text{(Eq. 3.6)}$$

$$\dot{q}_{conv.back} = h_{back}(T_{gas.back} - T_{back}) \qquad \text{(Eq. 3.7)}$$

where T_{back} is the temperature of the back sample surface, σ is the Stefan-Boltzmann constant, ε is emissivity of the paint used to coat the copper foil supporting the sample, and h_{back} = 4 W m^{-2} K^{-1} – a convective heat transfer coefficient determined in a previous study of CAPA II heat transfer [31]. Initial and final modeled back wall temperatures, $T_{gas.back.initial}$ and $T_{gas.back.final}$ as well as crossover time between the linear ramp and constant hold are shown in Table 3.6.

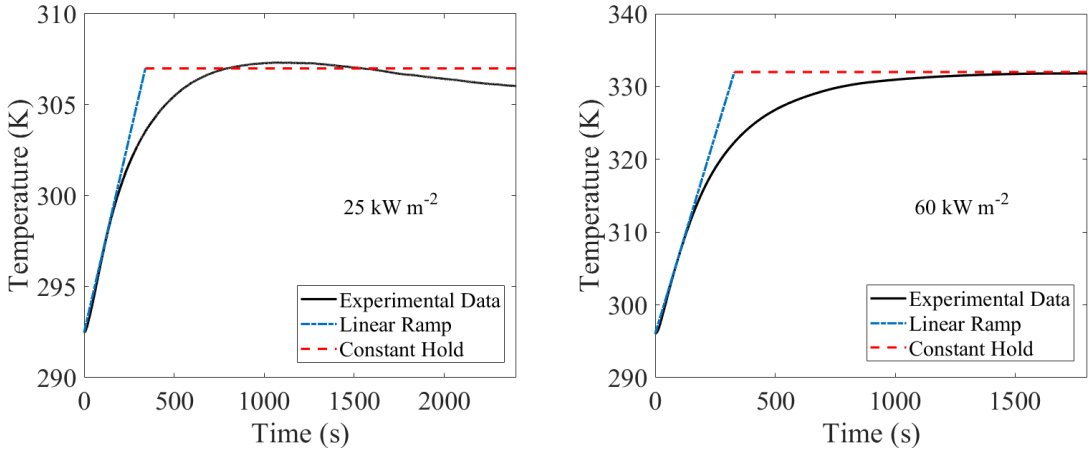

Fig. 3.18. *Modeled vs. experimental CAPA $T_{gas.back.}$ at 25 and 60 kW m^{-2}*

Table 3.6 *Modeled CAPA* $T_{gas.back.}$

Heat Flux	$T_{gas.back.initial}$ (K)	$T_{gas.back.final}$ (K)	*Crossover Time* (s)
25 kW m^{-2}	292.5	307	340
60 kW m^{-2}	296	332	330

Additional Model Assumptions

The emissivity and absorption coefficients of the virgin FPUF were assigned based on literature values [38,39] as 0.95 and 200 m^2 kg^{-1}, respectively. This absorption coefficient, which has been normalized by the foam density, essentially eliminates in depth absorption in the model. There is not much information available about the optical properties of Polyol or FPUF Residue, nor is the little information that is available necessarily applicable to the boiling, frothy condition of the components observed in the CAPA experiments. Therefore, the absorption coefficients and emissivities of the modeled Polyol and Residue components were initially assumed to be equal to that of the virgin FPUF.

All gaseous decomposition products were assumed not to contribute to sample volume [34], and were assumed to have a heat capacity of 2100 J kg^{-1} K^{-1}, which is the average heat capacity of a collection of C1 to C8 hydrocarbons at a temperature of 600 K. [40].

The densities of FPUF and Polyol were measured to be 28.7 kg m^{-3} and 700 kg m^{-3}, respectively. This is a somewhat low assignment of density for Polyol compared to typical values (~1000 kg m^{-3}) used in other studies.

Model Results

Initial model predictions did not capture the experimentally observed temperature or mass loss behavior, regardless of changes to the thermal conductivities of any component. Both back surface temperature and mass loss were significantly overpredicted. An investigation into the effects of changing other physical parameters was conducted, and it was found that only a reduction in the emissivity of Polyol could produce acceptable predictions. No changes to other physical parameters were effective. Therefore, the initial assumption that the optical properties of Polyol were identical to that of FPUF was eliminated. Instead, a manual optimization of Polyol emissivity was conducted (in conjunction with the automized optimization of the thermal conductivities of each reaction component).

Full optimizations of the thermal conductivities of each reaction component were conducted across a selection of Polyol emissivities ranging from 0.3-0.9. To add a degree of simplicity to the model, the emissivity and thermal conductivities of Polyol and Residue were set equal in each simulation. The 25 kW m^{-2} experiments were targeted for optimization but resulting 60 kW m^{-2} simulations are shown as well. The thermal conductivity of FPUF was optimized as a constant, while the thermal conductivity of the Polyol, and thereby the residue, was optimized as a linear function of temperature. The best obtainable fit of back surface temperature for each investigated modeled Polyol emissivity is shown in Figures 3.19 and 3.20. Legend labels correspond to the assigned Polyol and Residue emissivity for a model. An in-house script [32] was used to conduct the optimization. The goodness of fit criterion GoF that was targeted for the optimization was as described in Eq 3.8:

$$GoF_T = 1 - \sqrt{\frac{\sum_{i=1}^{N}\left(\frac{Exp_i - Model_i}{Exp_i}\right)^2}{N}}$$

where *Exp* indicates experimental values, *Model* indicates model values, and *N* is the number of experimental data points [32].

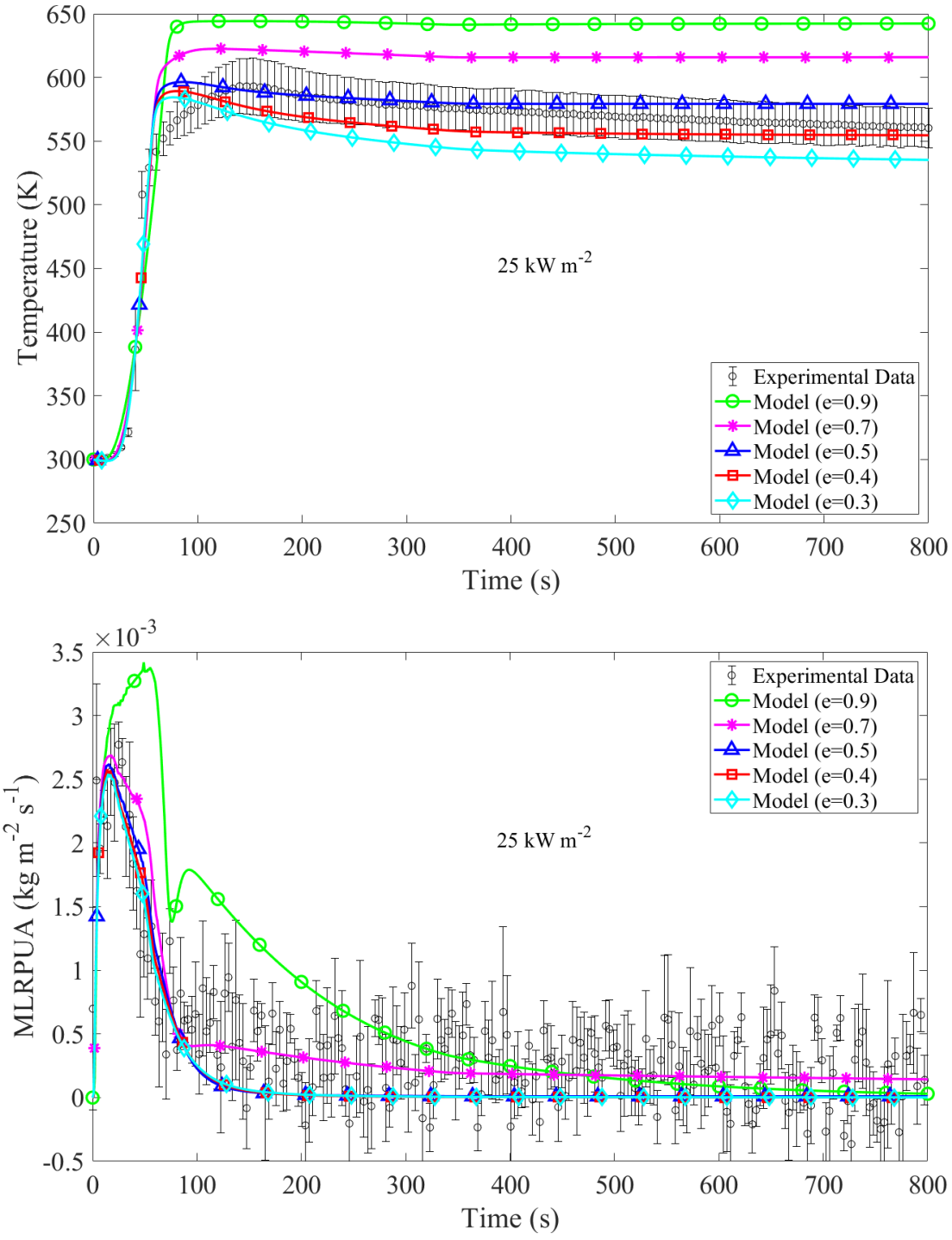

Fig. 3.19. *Modeled vs. experimental CAPA back surface temperature (top) and MLRPUA (bottom) for different assignments of emissivity to polyol and residue at 25 kW m^{-2}*

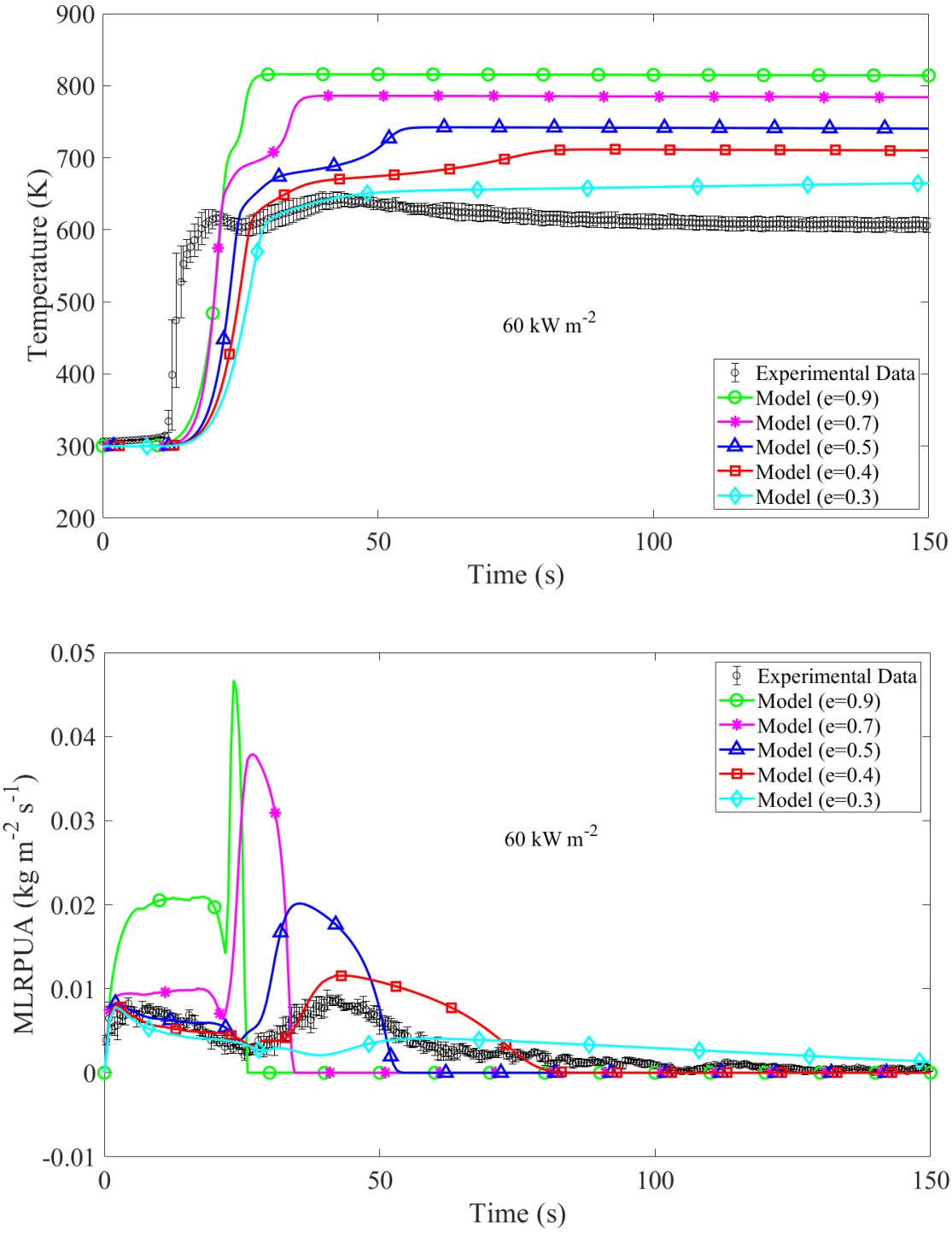

Fig. 3.20. *Modeled vs. experimental CAPA back surface temperature (top) and MLRPUA (bottom) for different assignments of emissivity to Polyol and residue at 60 kW m^{-2}*

The best fit resulted from an assigned emissivity of 0.4. This was the only emissivity that produced MLRPUA behavior which resembled experimental behavior at both heat fluxes, and which also captured the general behavior of the back surface temperature at the 25 kW m^{-2} flux. Even so, it did not necessarily capture the back surface temperature behavior at 60 kW m^{-2} well. The timing of the foam collapse is fairly well captured at 25 kW m^{-2} and slightly delayed compared to experimentally observed collapse at 60 kW m^{-2} (Fig 3.21). Isolated CAPA back surface temperature and MLRPUA results at this emissivity are shown in Figure 3.22. Resulting optimized thermal conductivities of each reaction component as well as the density and emissivity of each component are shown in Table 3.7. The optimized thermal conductivity of Polyol and Residue appears extremely high, but can be explained by the fact that it accounts for the bubbling/frothing/boiling behavior observed in experiments which greatly increases the heat transfer through the Polyol pool. It should not be thought of as purely a description of conductivity, but as a combined conductive/convective heat transfer term.

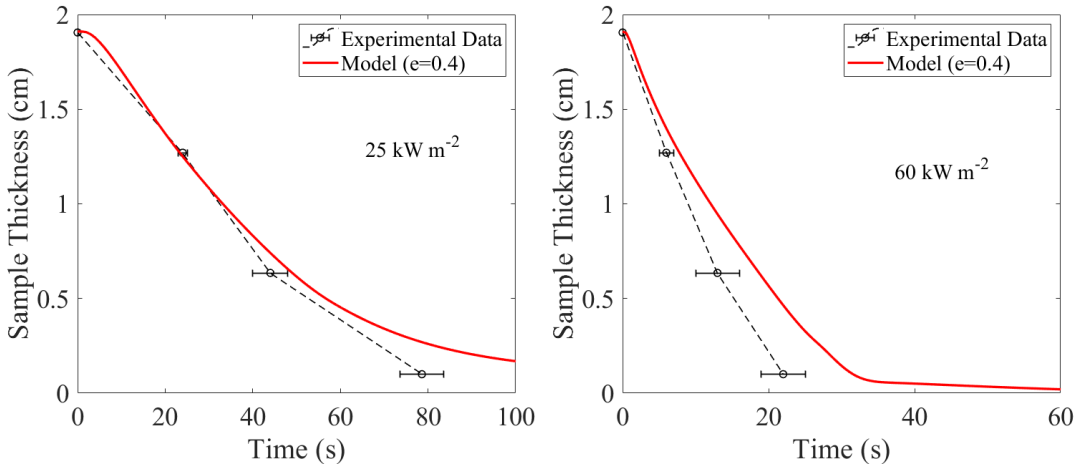

Fig. 3.21. *Experimentally observed sample thickness evolution vs. ThermaKin predictions*

It should be noted that the current CAPA II modeling results, shown in Figure 3.22, do not provide as good agreement with experiments as was demonstrated in previous studies for various combustible solids [27,30,32,37]. Both the low initial density of FPUF and rapid and large (more than an order of magnitude) increase in density of the foam upon decomposition to Polyol present a unique challenge for the model parameterization. Nevertheless, to our knowledge, the current model of FPUF is the most validated comprehensive pyrolysis model available.

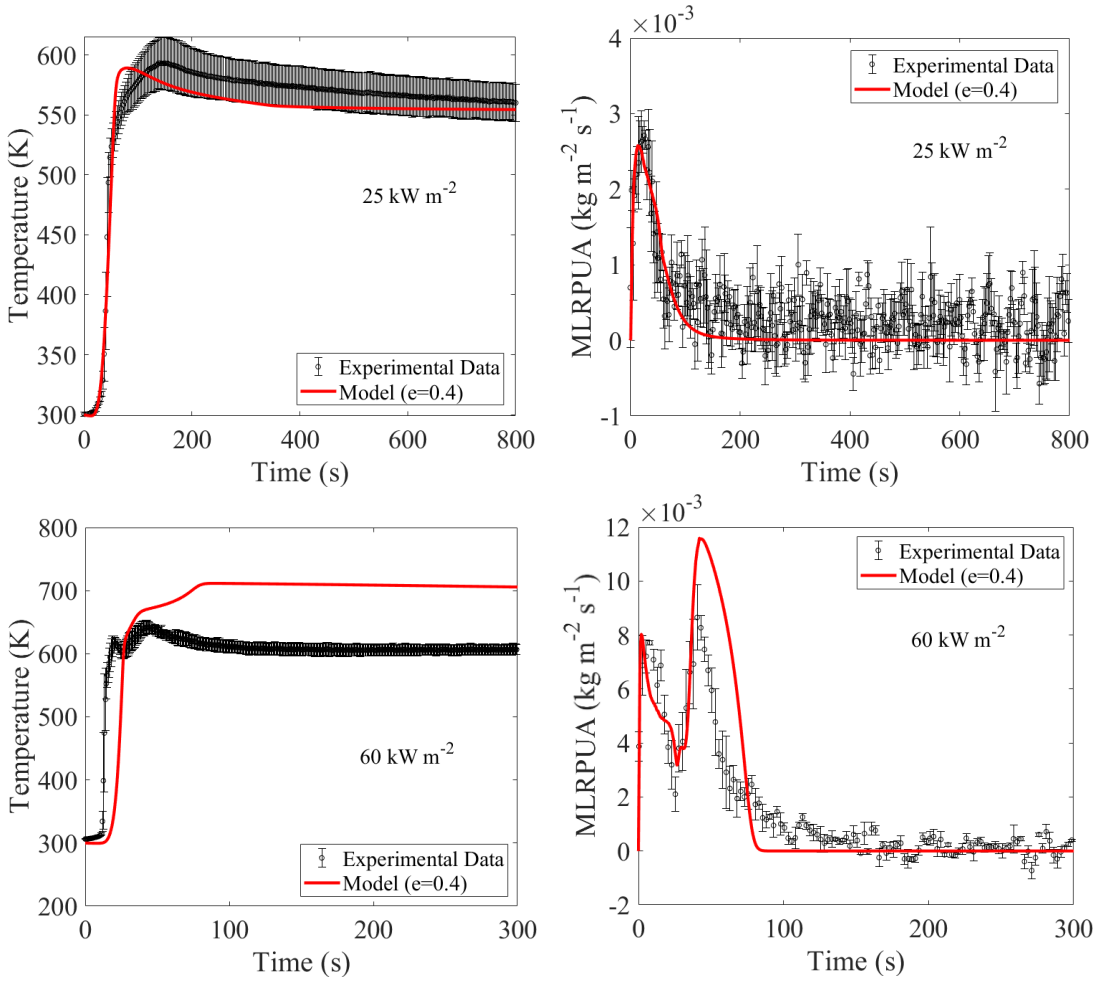

Fig. 3.22. *Modeled vs. experimental CAPA MLRPUA and back surface temperature for the best fit assignment of emissivity to polyol and residue (0.4) at 25 kW m^{-2} (top) 60 kW m^{-2} (bottom)*

Table 3.7. *Final component properties determined from CAPA modeling*

Component	*Thermal Conductivity* (W m^{-1} K^{-1})	*Density* (kg m^{-3})	*Emissivity*
FPUF	0.0735	28.7	0.95
Polyol & Residue	$0.1 + 0.485 \times T$	700	0.4

Chapter 4: Conclusions and Future Work

TGA, DSC, MCC, and CAPA II experiments were performed on a non-fire-retarded FPUF to develop a comprehensive pyrolysis model. Experimental data was inversely analyzed with ThermaKin2Ds to obtain reaction kinetics and thermodynamics parameters, complete heats of combustion, and thermal conductivities of components associated with the anaerobic pyrolysis of FPUF. Modeled TGA, DSC, and MCC data agreed well with experimental results and confidence is high that the resulting decomposition kinetics parameters, thermodynamics parameters, and complete heats of combustion of gaseous components that were obtained for the pyrolysis are accurate. Agreement of the modeled CAPA II data with experimentally observed behavior is acceptable but not as good as was achieved in previous studies of other combustible solids. Optical properties of the FPUF decomposition reaction products are not available and hard to measure. Future work should focus on probing these optical properties through more direct measurements and testing performance of the current model in different, preferably larger scale fire scenarios.

References

[1] NFPA, Ahrens, M., & Maheshwari, R. (2020, November). Home Structure Fires. https://www.nfpa.org//-/media/Files/News-and-Research/Fire-statistics-and-reports/Building-and-life-safety/oshomes.pdf

[2] Gama NV, Ferreira A, Barros-Timmons A. Polyurethane Foams: Past, Present, and Future. Materials. 2018; 11(10):1841. https://doi.org/10.3390/ma11101841

[3] Drysdale, D. (2012). Fundamentals of the Fire Behaviour of Cellular Polymers. In Fire and Cellular Polymers (p. 61). Springer Publishing.

[4] Morgan AB. Revisiting flexible polyurethane foam flammability in furniture and bedding in the United States. Fire and Materials. 2021;45:68–80.https://doi.org/10.1002/fam.284880

[5] State of California Department of Consumer Affairs. (2013, January). Requirements, Test Procedure and Apparatus for Testing the Smolder Resistance of Materials Used in Upholstered Furniture (No. TB117-2013). https://www.gsa.gov/cdnstatic/TB_117_2013.pdf

[6] US Consumer Product Safety Commission. (2006). Laboratory Test Manual For 16 C.F.R. Part 1632: Standard for the Flammability of Mattresses and Mattress Pads. https://www.cpsc.gov/s3fs-public/pdfs/blk_media_testmatt.pdf

[7] Kashiwagi, T. (1994). Polymer combustion and flammability—Role of the condensed phase. Symposium (International) on Combustion, 25(1), 1423–1437. https://doi.org/10.1016/s0082-0784(06)80786-1

[8] K. Mcgrattan, S. Hostikka, R. Mcdermott, J. Floyd, C. Weinschenk, K. Overholt, Sixth Edition Fire Dynamics Simulator Technical Reference Guide Volume 4: Configuration Management, 4 (2017). doi:10.6028/NIST.SP.1018-4.

[9] C. Lautenberger, C. Fernandez-Pello, Generalized pyrolysis model for combustible solids, Fire Saf. J. 44 (2009) 819–839. doi:10.1016/j.firesaf.2009.03.011.

[10] S.I. Stoliarov, R.E. Lyon, Thermo-Kinetic Model of Burning for Pyrolyzing Materials, in: Fire Saf. Sci. - Proc. 9th Int. Symp., 2008: pp. 1141–1152. doi:10.3801/IAFSS.FSS.9-1141.

[11] Korobeinichev, O., Gonchikzhapov, M., Tereshchenko, A., Gerasimov, I., Shmakov, A., Paletsky, A., & Karpov, A. (2018). An experimental study of horizontal flame spread over PMMA surface in still air. Combustion and Flame, 188, 388–398. https://doi.org/10.1016/j.combustflame.2017.10.008

[12] Krämer, R., Zammarano, M., Linteris, G., Gedde, U., & Gilman, J. (2010). Heat release and structural collapse of flexible polyurethane foam. Polymer Degradation and Stability, 95(6), 1115–1122. https://doi.org/10.1016/j.polymdegradstab.2010.02.019

[13] Lefebvre, J., Bastin, B., Le Bras, M., Duquesne, S., Paleja, R., & Delobel, R. (2005). Thermal stability and fire properties of conventional flexible polyurethane foam formulations. Polymer Degradation and Stability, 88(1), 28–34. https://doi.org/10.1016/j.polymdegradstab.2004.01.025

[14] Rein, G., Lautenberger, C., Fernandezpello, A., Torero, J., & Urban, D. (2006). Application of genetic algorithms and thermogravimetry to determine the kinetics of polyurethane foam in smoldering combustion. Combustion and Flame, 146(1–2), 95–108. https://doi.org/10.1016/j.combustflame.2006.04.013

[15] Lautenberger, C., & Fernandez-Pello, A. (2011). Optimization Algorithms for Material Pyrolysis Property Estimation. Fire Safety Science, 10, 751–764. https://doi.org/10.3801/iafss.fss.10-751

[16] Dodd, A. B., Lautenberger, C., & Fernandez-Pello, A. C. (2009). Numerical examination of two-dimensional smolder structure in polyurethane foam. Proceedings of the Combustion Institute, 32(2), 2497-2504.

[17] Pau, D., Fleischmann, C., & Delichatsios, M. (2020). Thermal decomposition of flexible polyurethane foams in air. Fire Safety Journal, 111, 102925. https://doi.org/10.1016/j.firesaf.2019.102925

[18] Viswanath, S., & Gupta, M. (1996). Estimation of nonisothermal kinetic parameters from a TG curve by the methods of overdetermined system and inflection point. Thermochimica Acta, 285(2), 259–267. https://doi.org/10.1016/0040-6031(96)02917-6

[19] Pau, D. S., Fleischmann, C. M., Spearpoint, M. J., & Li, K. Y. (2013). Determination of kinetic properties of polyurethane foam decomposition for pyrolysis modelling. Journal of Fire Sciences, 31(4), 356–384. https://doi.org/10.1177/0734904113475858

[20] Friedman, H. L. (1964). Kinetics of thermal degradation of char-forming plastics from thermogravimetry. Application to a phenolic plastic. Journal of Polymer Science Part C: Polymer Symposia, 6(1), 183–195. https://doi.org/10.1002/polc.5070060121

[21] Bilbao, R., Mastral, J., Ceamanos, J., & Aldea, M. (1996). Kinetics of the thermal decomposition of polyurethane foams in nitrogen and air atmospheres. Journal of Analytical and Applied Pyrolysis, 37(1), 69–82. https://doi.org/10.1016/0165-2370(96)00936-9

[22] Li, K., Pau, D. S., & Zhang, H. (2015). Pyrolysis of polyurethane foam: optimized search for kinetic properties via simultaneous K-K method, genetic algorithm and elemental analysis. Fire and Materials, 40(6), 800–817. https://doi.org/10.1002/fam.2343

[23] Prasad, K. , Kramer, R. , Marsh, N. , Nyden, M. , Ohlemiller, T. , Pitts, W. and Zammarano, M. (2009), NUMERICAL SIMULATION OF FIRE SPREAD ON POLYURETHANE FOAM SLABS, Proceedings of the Fire and Materials Conference, San Francisco, CA, [online], https://tsapps.nist.gov/publication/get_pdf.cfm?pub_id=901154 (Accessed May 7, 2021)

[24] Stoliarov, S. I., & Li, J. (2016). Parameterization and Validation of Pyrolysis Models for Polymeric Materials. *Fire Technology*, *52*(1), 79–91. https://doi.org/10.1007/s10694-015-0490-1

[25] Li, J., & Stoliarov, S. I. (2013). Measurement of kinetics and thermodynamics of the thermal degradation for non-charring polymers. Combustion and Flame, 160(7), 1287–1297. https://doi.org/10.1016/j.combustflame.2013.02.012

[26] Li, J., & Stoliarov, S. I. (2014). Measurement of kinetics and thermodynamics of the thermal degradation for charring polymers. Polymer Degradation and Stability, 106, 2–15. https://doi.org/10.1016/j.polymdegradstab.2013.09.022

[27] McKinnon, M., & Stoliarov, S. (2015). Pyrolysis Model Development for a Multilayer Floor Covering. Materials, 8(9), 6117–6153. https://doi.org/10.3390/ma8095295

[28] Li, J., Gong, J., & Stoliarov, S. I. (2014). Gasification experiments for pyrolysis model parameterization and validation. International Journal of Heat and Mass Transfer, 77, 738–744. https://doi.org/10.1016/j.ijheatmasstransfer.2014.06.003

[29] Li, J., Gong, J., & Stoliarov, S. I. (2015). Development of pyrolysis models for charring polymers. *Polymer Degradation and Stability*, *115*, 138–152. https://doi.org/10.1016/j.polymdegradstab.2015.03.003

[30] Ding, Y., Swann, J. D., Sun, Q., Stoliarov, S. I., & Kraemer, R. H. (2019). Development of a pyrolysis model for glass fiber reinforced polyamide 66 blended with red phosphorus: Relationship between flammability behavior and material composition. Composites Part B: Engineering, 176, 107263. https://doi.org/10.1016/j.compositesb.2019.107263

[31] Swann, J. D., Ding, Y., McKinnon, M. B., & Stoliarov, S. I. (2017). Controlled atmosphere pyrolysis apparatus II (CAPA II): A new tool for analysis of pyrolysis of charring and intumescent polymers. Fire Safety Journal, 91, 130–139. https://doi.org/10.1016/j.firesaf.2017.03.038

[32] Fiola, G. J. (2019). Improving inverse analysis of pyrolysis model parameterization using hill climbing algorithms (Thesis). http://hdl.handle.net/1903/25419

[33] Stoliarov, S. I., Leventon, I. T., & Lyon, R. E. (2013). Two-dimensional model of burning for pyrolyzable solids. Fire and Materials, 38(3), 391–408. https://doi.org/10.1002/fam.2187

[34] Swann, J. D., Ding, Y., & Stoliarov, S. I. (2019). Characterization of pyrolysis and combustion of rigid poly(vinyl chloride) using two-dimensional modeling. International Journal of Heat and Mass Transfer, 132, 347–361. https://doi.org/10.1016/j.ijheatmasstransfer.2018.12.011

[35] ASTM International, D7309-11 Standard Test Method for Determining Flammability Characteristics of Plastics and Other Solid Materials Using Microscale Combustion Calorimetry, West Conshohocken, 2011. doi:10.1520/D7309-11.

[36] Ravey, M., & Pearce, E. M. (1997). Flexible polyurethane foam. I. Thermal decomposition of a polyether-based, water-blown commercial type of flexible polyurethane foam. Journal of Applied Polymer Science, 63(1), 47–74.

[37] Swann, J. (2019). A COMPREHENSIVE CHARACTERIZATION OF PYROLYSIS AND COMBUSTION OF INTUMESCENT AND CHARRING POLYMERS USING TWO-DIMENSIONAL MODELING: A RELATIONSHIP BETWEEN THERMAL TRANSPORT AND THE PHYSICAL STRUCTURE OF THE INTUMESCENT CHAR. https://drum.lib.umd.edu/handle/1903/21906

[38] Chen, J., Zhou, Y., Nan, Q., Sun, Y., Ye, X., & Wang, Z. (2007). Synthesis, characterization and infrared emissivity study of polyurethane/TiO2 nanocomposites. Applied Surface Science, 253(23), 9154–9158. https://doi.org/10.1016/j.apsusc.2007.05.046

[39] Ferkl, P., Toulec, M., Laurini, E., Pricl, S., Fermeglia, M., Auffarth, S., Eling, B., Settels, V., & Kosek, J. (2017). Multi-scale modelling of heat transfer in polyurethane foams. Chemical Engineering Science, 172, 323–334. https://doi.org/10.1016/j.ces.2017.06.035

[40] Linstrom, P. J., & Mallard, W. G. (2001). The NIST Chemistry WebBook: A Chemical Data Resource on the Internet†. Journal of Chemical & Engineering Data, 46(5), 1059–1063. https://doi.org/10.1021/je000236i

[41] McKinnon, M., & Stoliarov, S. (2015b). Pyrolysis Model Development for a Multilayer Floor Covering. Materials, 8(9), 6117–6153. https://doi.org/10.3390/ma8095295